Variable Features on Mars, 2, Mariner 9 Global Results

C. SAGAN, J. VEVERKA, P. FOX, R. DUBISCH, R. FRENCH, AND P. GIERASCH

Laboratory for Planetary Studies, Cornell University, Ithaca, New York 14850

L. QUAM, J. LEDERBERG, E. LEVINTHAL, R. TUCKER, AND B. EROSS

Artificial Intelligence Laboratory and Department of Genetics, Stanford Medical School Stanford University, Stanford, California 94305

J. B. POLLACK

NASA Ames Research Center, Moffett Field, California 94035

Systematic Mariner 9 monitoring of the space and time distribution of Martian bright and dark markings, the streaks and splotches, indicates a range of global correlations. The time-variable classical dark markings owe their configurations and variability to their constituent streaks and splotches, produced by windblown dust. Streaks and splotches are consistent wind direction indicators. Correlation of global streak patterns with general circulation models shows that velocities ~50 to 90 m/sec above the boundary layer are necessary to initiate grain motion on the surface and to produce streaks and splotches. Detailed examples of changes in Syrtis Major, Lunae Palus, and Promethei Sinus are generally consistent with removal of bright sand and dust and uncovering of darker underlying material as the active agent in such changes, although dark mobile material probably also exists on Mars. The generation of streaks and the progressive albedo changes observed require only threshold velocities of about 2 m/sec for about 1 day at the grain surface. We propose that the dark collar observed following the north polar cap in its retreat is produced by the scouring of bright overlying dust from the polar peripheral ground by winds driven by the temperature differences between frosted and unfrosted terrain. The stability of bright streaks and the variability of dark streaks and splotches, as well as their contrast, can be the result of size differences of the constituent particles.

One of the principal objectives of the Mariner 9 mission was to examine, at high resolution and extended time baseline, the surface albedo variations on Mars. The preliminary results of this investigation have been presented by *Sagan et al.* [1972; here called paper 1]. The time-variable Martian dark areas and representative semitone areas were found commonly to be resolved into two kinds of fine structure: streaks and splotches. Most streaks emanate from craters, although some begin at positive relief features. Bright streaks tend to be long and narrow; dark streaks, shorter and broader. Typical streak lengths are tens of kilometers. Splotches are irregular markings that exhibit a significant tendency to be located inside craters, often asymmetrically against a crater wall. Larger splotches may wash over crater ramparts onto adjoining terrain.

A large variety of splotches and streaks have been systematically observed during the mission. In many cases, all three photometric angles were held nearly constant so that true variations in the albedo of these markings could be separated from changes in shadows and the effects of the surface scattering function. These observations were designed to detect relative albedo changes within the field of view. No conclusions are based on absolute photometry. Major variations in splotches and dark streaks were uncovered with a characteristic time scale for variations of ≤ 2 weeks. Variations on a

time scale of 1 day were sought; such rapid variations must be relatively uncommon, as none were discovered. No variations of bright streaks, either in production or dissipation, were found. In several places, most notably Syrtis Major, the configuration of dark and bright streaks corresponds remarkably well to the classical earth-based configuration of the dark area that the streaks constitute. Observed time variations in the distribution of such streaks correspond to regions in which the albedo variations were previously observed from earth. Paper 1 proposed that the distribution and time variation of streaks and splotches are the causes of the classical seasonal and secular variations of Martian albedo markings.

Two principal hypotheses were proposed in pre-Mariner 9 days to explain these variations: biology and windblown dust. Although convincing evidence against biological explanations are not forthcoming, mainly because a wide range of properties can be proposed for hypothetical Martian organisms, the evidence of paper 1 is strongly in favor of windblown dust producing streaks and splotches and their time variations. A range of explanations of the streaks and splotches was mentioned in paper 1. For example, bright streaks might be produced by bright dust trapped in negative relief dust sinks (such as crater bottoms) in the waning stages of the dust storm, and subsequently deflated by strong gusts. Or fine dust deposited uniformly by a dust storm may subsequently be stirred up, suspended, and blown away because of collisions with saltating grains everywhere but in the lee of crater walls, where the wind velocities are low. Examples of both of these cases on a smaller scale are known in Antarctic dry valleys [*Morris et al.*, 1972]. Alternatively, dust darker than the mean albedo of a given area might be layered down by the wind from a prevailing direction everywhere but in the lee of crater ramparts. But in these cases, as with other explanations of the streaks, they will point in the direction of the wind flow. Thus it was proposed in paper 1 that the streaks may be natural wind vanes and possibly anemometers placed on the Martian surface.

In this paper, we present global maps of the streaks, streak-splotch correlations, and a comparison of wind flow patterns deduced from these maps with results on the general circulation of the Martian atmosphere. We derive a new estimate of the wind velocities necessary to initiate dust movement on the Martian surface, exhibit detailed examples of variations in three regions of Mars, and present new conclusions on the mechanisms of wind-initiated albedo changes.

GLOBAL STREAK MAPS

The entire surface of Mars was mapped for streaks, both bright and dark. Mapping was based primarily on Ozalid mosaics of wide-angle pictures prepared by the Astrogeology Branch, U.S. Geological Survey. These pictures are a convenient source, allowing easy mapping of streaks that traverse wide-angle picture boundaries, but they also limited our effective minimum detectable streak length to about 10 km. There are many smaller streaks on narrow-angle pictures, but Mariner 9 did not provide adequate narrow-angle coverage of Mars to permit useful high-resolution streak mapping. The mosaics cover the time interval between revolutions 101 and 222, corresponding to $L_s = 320°$ to 353°, or late summer in the southern hemisphere. Our results apply only to this season.

Quite different results may apply to other seasons, inasmuch as only the appearance of dark streaks, never the removal of dark streaks nor the appearance of bright streaks, was observed during this time interval. Such a situation cannot continue indefinitely if Mars is to maintain the general appearance to earth that it has exhibited for more than a century. On the other hand, the frequency of alteration of streaks observed must represent some integration of streaks produced recently and streaks produced at some more remote times, perhaps of the order of 1 year in the past.

Streaks were mapped by four coauthors of this paper, and there was significant overlap among their counts to guarantee no major personal systematic errors. The relative number of marginal streaks proved to be few, primarily cases on the border between short streaks and long splotches spilling over crater walls. The final streak maps were carefully proofed against the original compilations. In the present study, we are concerned only with the weather vane, not with the hypothesized anemometer, aspect of the streaks. Accordingly streak lengths are

displayed on two scales: the short
spond to streaks $\leq$60 km long; the
correspond to streaks $\geq$60 km
streaks are represented by solid a
streaks by dashed arrows. The re
played in Figure 1 in Lambert co
Mercator maps. There are area
number of parallel streaks was s
given small area that representa
streak on maps of this scale woul
impossible (cf. paper 1, Figure 1
regions of great arrow density, o
sentative sampling of streaks is i
loss in generality for streak dire
from this convention.

Figures 2 and 3 show the streaks
projection on earth-based albedo
9 topographic maps, respectively. T
of the north polar hood and an ap
paucity of streaks in the south
region for the L_s of these observ
reason for the blank areas in th
the absence of streak maps for r
of −65°. In Figures 2 and 3, only t
streak direction within each 10°
square is shown. Where there are tw
directions, both are shown. As is
the rosette diagram for the Solis
(Figure 4), one or two prevailing d
almost always a good approxima
there is a notably high density of
grid square, it is represented by a
Wind directions have been plotte
bright and dark streaks, which in s
give concordant and in other region
directions, probably because they
produced at different times.

IMPLICATIONS OF THE STREAK

We have previously shown (pap
16) that the configuration of Sy
corresponds well to the distributi
stituent dark streaks. In Figure 5
plot the distribution of streaks in
of Solis Lacus, a well-known se
secular variable. The earth-based
Solis Lacus, circa 1969, after the
servatory cartography, also is sh
sidering the variability of this f
agreement between the classical c
and the locus of streaks is excellent
with our previous conclusions. We p

displayed on two scales: the short arrows correspond to streaks ≤ 60 km long; the long arrows correspond to streaks ≥ 60 km long. Dark streaks are represented by solid arrows, bright streaks by dashed arrows. The results are displayed in Figure 1 in Lambert conformal and Mercator maps. There are areas where the number of parallel streaks was so great in a given small area that representation of each streak on maps of this scale would have been impossible (cf. paper 1, Figure 16). In such regions of great arrow density, only a representative sampling of streaks is indicated. No loss in generality for streak direction results from this convention.

Figures 2 and 3 show the streaks in Mercator projection on earth-based albedo and Mariner 9 topographic maps, respectively. The existence of the north polar hood and an apparently real paucity of streaks in the south circumpolar region for the L_s of these observations is the reason for the blank areas in the north and the absence of streak maps for regions south of $-65°$. In Figures 2 and 3, only the prevailing streak direction within each $10° \times 10°$ grid square is shown. Where there are two prevailing directions, both are shown. As is indicated in the rosette diagram for the Solis Lacus region (Figure 4), one or two prevailing directions are almost always a good approximation. Where there is a notably high density of streaks in a grid square, it is represented by a thick arrow. Wind directions have been plotted for both bright and dark streaks, which in some regions give concordant and in other regions discordant directions, probably because they have been produced at different times.

Implications of the Streak Maps

We have previously shown (paper 1, Figure 16) that the configuration of Syrtis Major corresponds well to the distribution of constituent dark streaks. In Figure 5 we similarly plot the distribution of streaks in the vicinity of Solis Lacus, a well-known seasonal and secular variable. The earth-based outline of Solis Lacus, circa 1969, after the Lowell Observatory cartography, also is shown. Considering the variability of this feature, the agreement between the classical configuration and the locus of streaks is excellent, consistent with our previous conclusions. We propose that marked secular changes in Solis Lacus [e.g., *Antoniadi*, 1930, p. 140] are due to extraordinary wind regimes, redistributing fine dust in this area. Other factors being equal, small dark regions surrounded on all sides by bright areas should be more susceptible to eolian secular changes [*Pollack and Sagan*, 1967]. Ultimately a reconstruction of several different wind regimes, a kind of eolian stratigraphy, should be possible from data such as that exhibited in Figure 5. We return to this subject elsewhere.

In addition to specific cases, such as Syrtis Major and Solis Lacus, we see from Figure 2 that the global distribution of streaks corresponds well to the general configuration of dark areas as viewed from earth. In these figures there are many cases where two different flow directions are in evidence. We interpret these as the remnants of the flow regimes in the Martian atmosphere at two different epochs, probably two different seasons. It also is possible that a subset of flow directions belongs to the great 1971 dust storm and is not typical of wind patterns in the absence of global storm systems.

In the latitude band between 20°N and 20°S (regions MC-8 to MC-23) there is a clear tendency for the flow to be from the NE north of the equator and from the NW south of the equator. This pattern corresponds to the zonally averaged surface wind calculated by *Leovy and Mintz* [1969] for southern hemisphere summer. It also appears in the wind field maps derived from the Mariner 9 infrared interferometer spectrometer (Iris) experiment (Figure 6). The Iris wind fields are determined from the pressure-temperature profiles obtained by inversion of the infrared emission spectrum. The results above the surface boundary layer displayed in Figure 6 were derived by J. A. Pirraglia [cf. *Hanel et al.*, 1972; *Conrath et al.*, 1973] from temperatures during the dust storm. An approximate dynamical theory is used. It is especially important for our purposes that: (1) topography is neglected, and (2) the results are most uncertain close to the equator. Winds at the equator are probably overestimated. The general configuration of the flow pattern is probably correct, however, and the agreement between the calculated winds and the streak

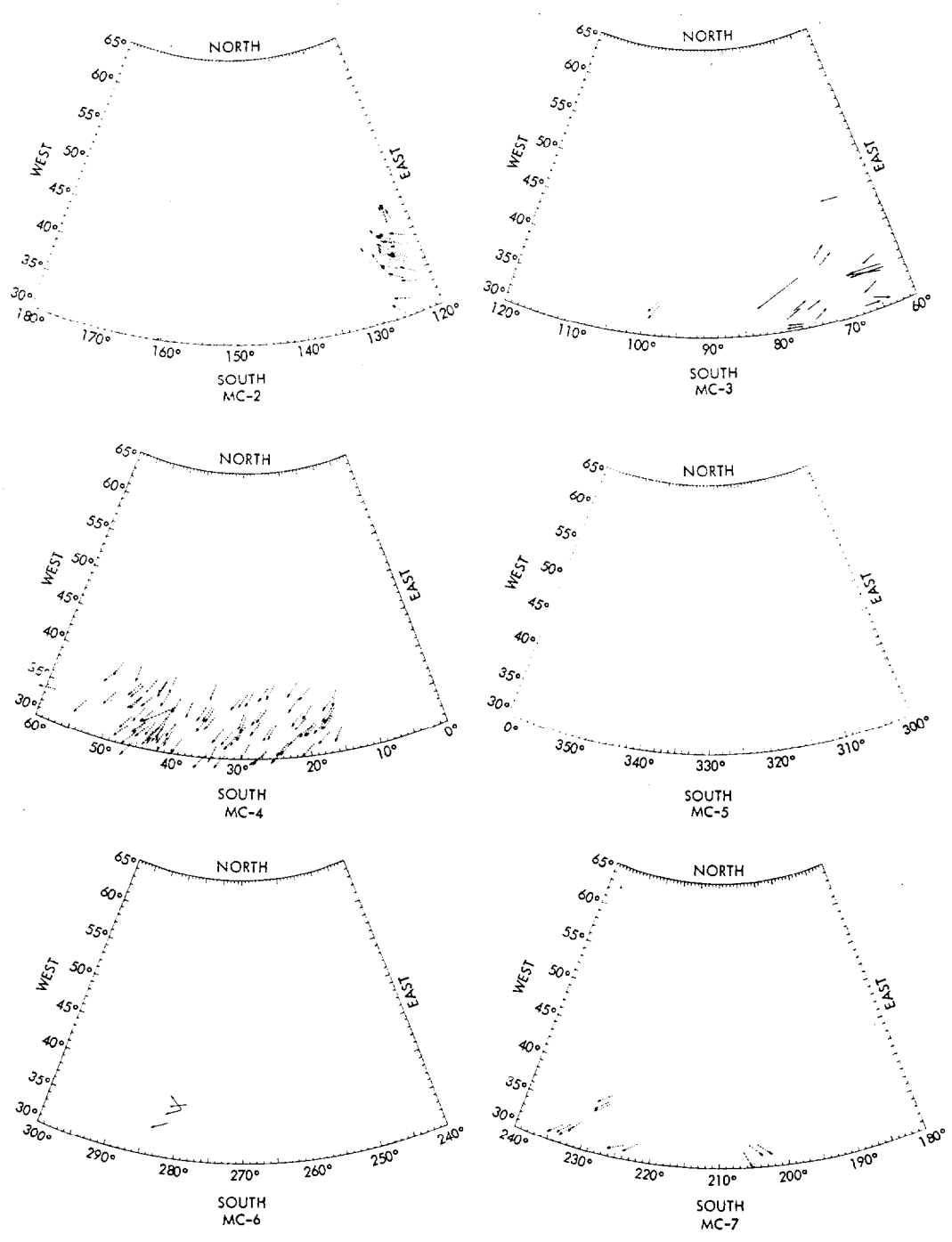

Fig. 1. Streak maps of Mars. Solid arrows represent dark streaks; dashed arrows represent bright streaks. The arrow length is about four times the streak length, but is approximate. The shortest arrows shown (2° of latitude long) represent streaks $\lesssim$60 km in length. Regions of the planet north of 50°N could not be mapped for streaks because of obscuration by the polar hood. The absence of streaks in these regions, evident in Figures 1 and 2, may not be real.

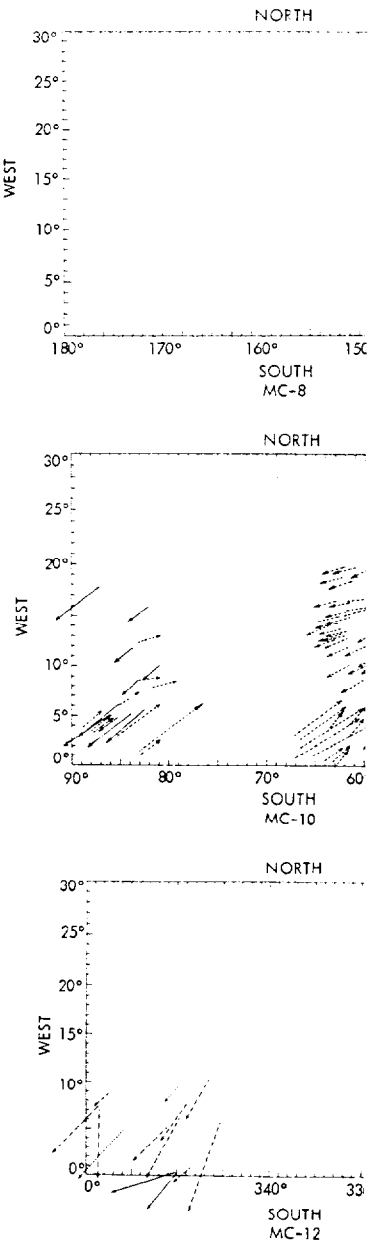

orientations in the latitude b
remarkably good.

At equatorial latitudes the ca
are strongest and are practical
higher latitudes their magnitude
the direction varies during a
Pirraglia's calculation isolates t
steady winds from the diurnally

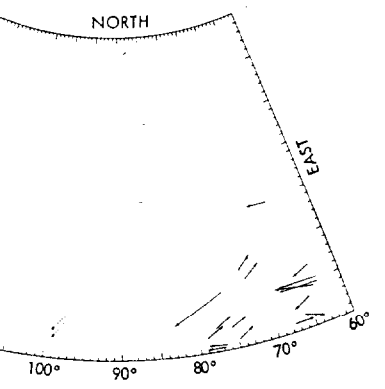

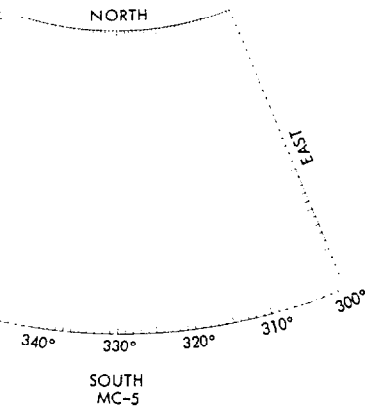

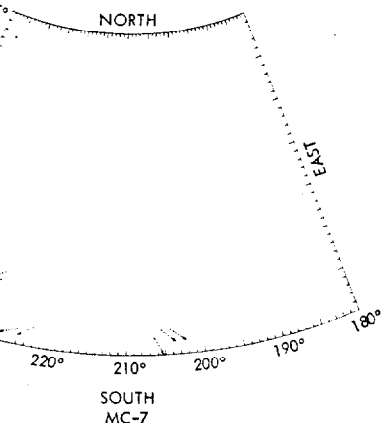

streaks; dashed arrows represent
reak length, but is approximate.
reaks ≲60 km in length. Regions
ts because of obscuration by the
in Figures 1 and 2, may not be

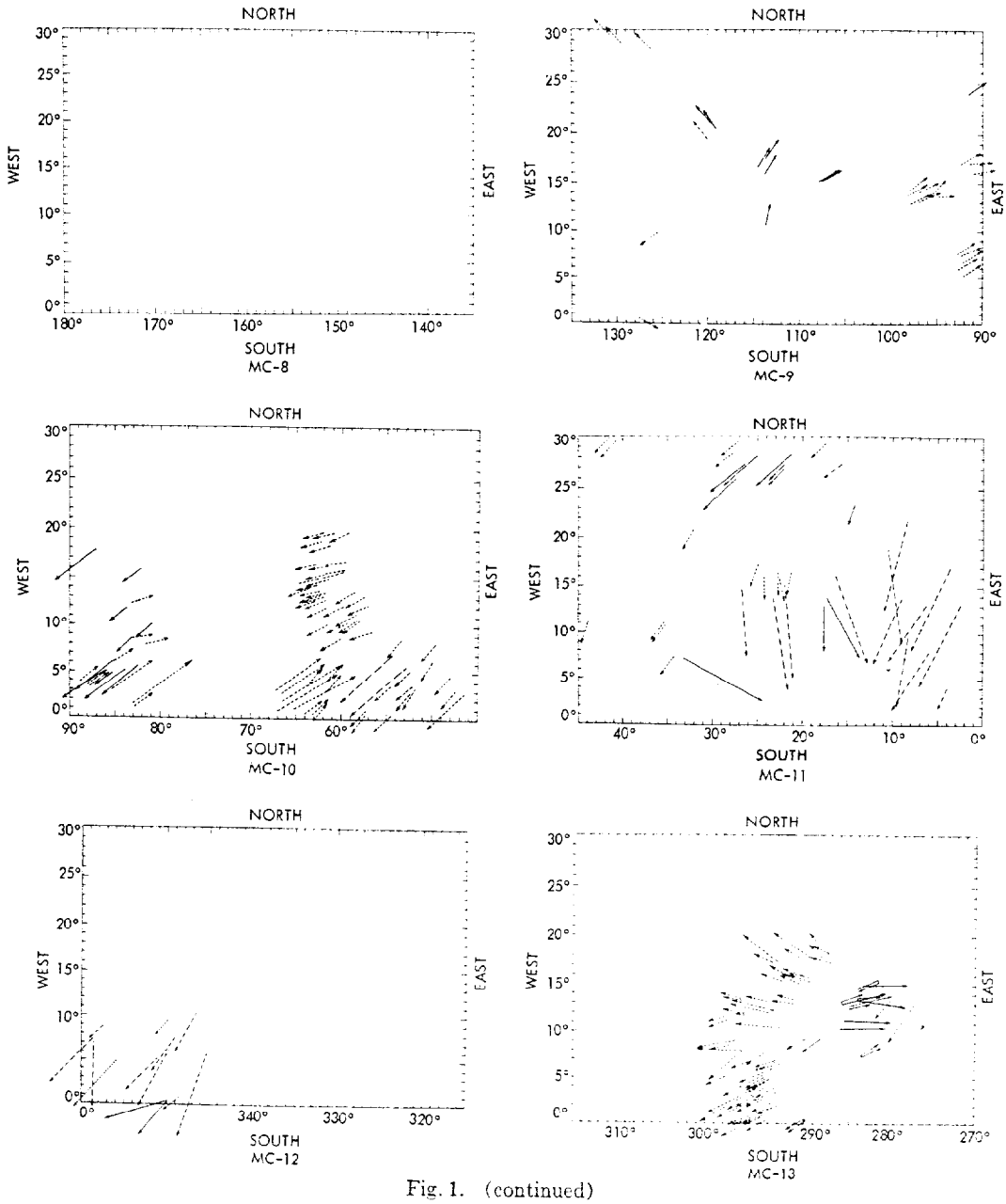

Fig. 1. (continued)

orientations in the latitude band ±20° is remarkably good.

At equatorial latitudes the calculated winds are strongest and are practically steady. At higher latitudes their magnitudes are less and the direction varies during a diurnal cycle. Pirraglia's calculation isolates the large-scale steady winds from the diurnally varying winds. We know that there is a range of other winds expected on Mars, including slope and obstacle winds driven by the large elevation differences [*Gierasch and Sagan*, 1971; *Sagan et al.*, 1971; *Blumsack*, 1971] and winds driven by the large temperature gradient between frosted and unfrosted polar ground [*Leovy et al.*, 1973]. We might expect such winds to dominate at

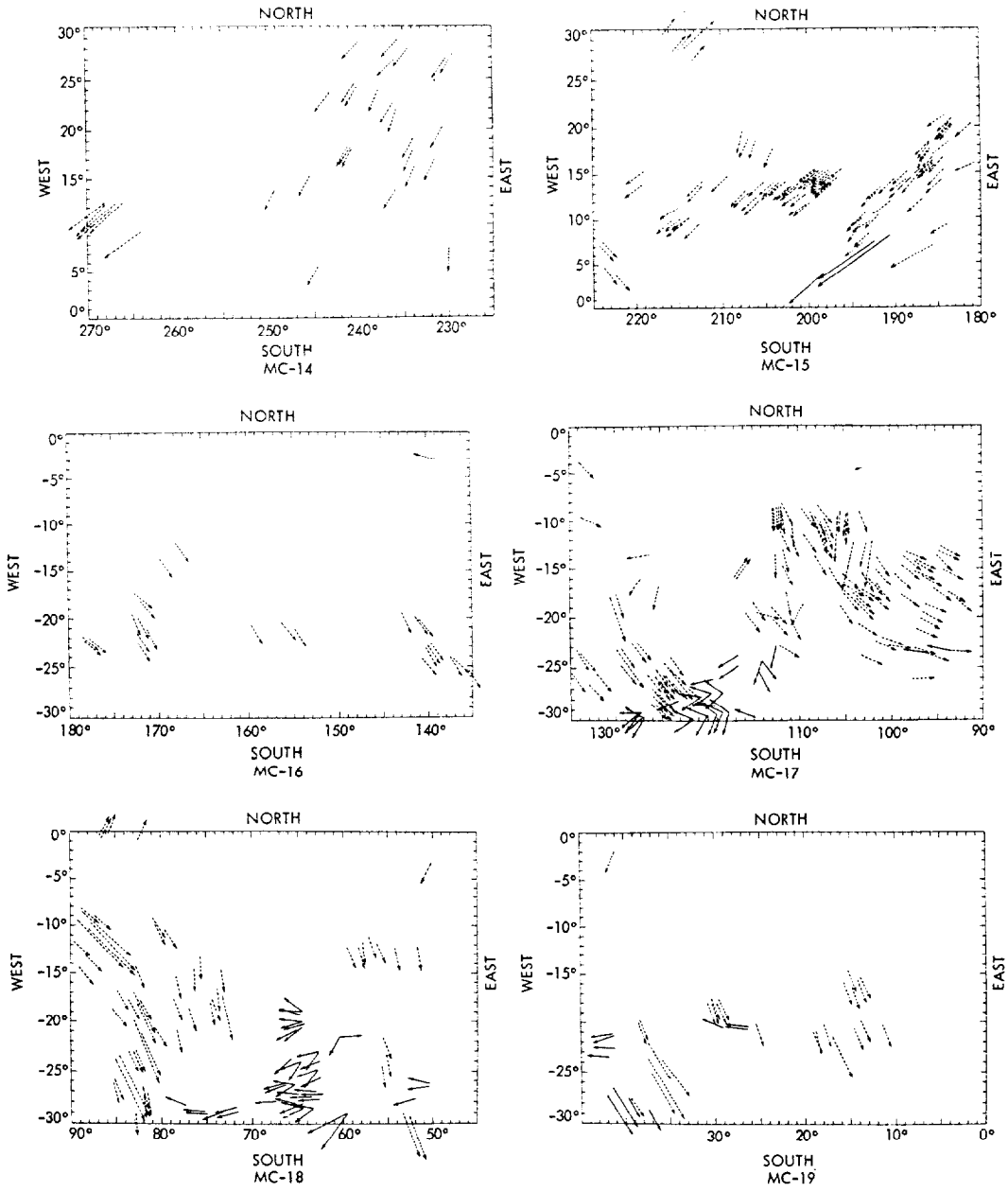

Fig. 1. (continued)

higher latitudes, and the steady component that Pirraglia calculates to dominate at low latitudes.

The streak maps (Figures 1 to 3) support this contention. The flow indicated at high latitudes does not correspond to that predicted either by Pirraglia or by Leovy and Mintz. An interesting regularity at higher latitude is the indication of a steady easterly flow component at latitudes 20° to 40°S. This is the latitude range and initial direction of flow of the great 1971 global dust storm, and it is possible that this flow component is a marker of that storm.

Other peculiarities may be connected with

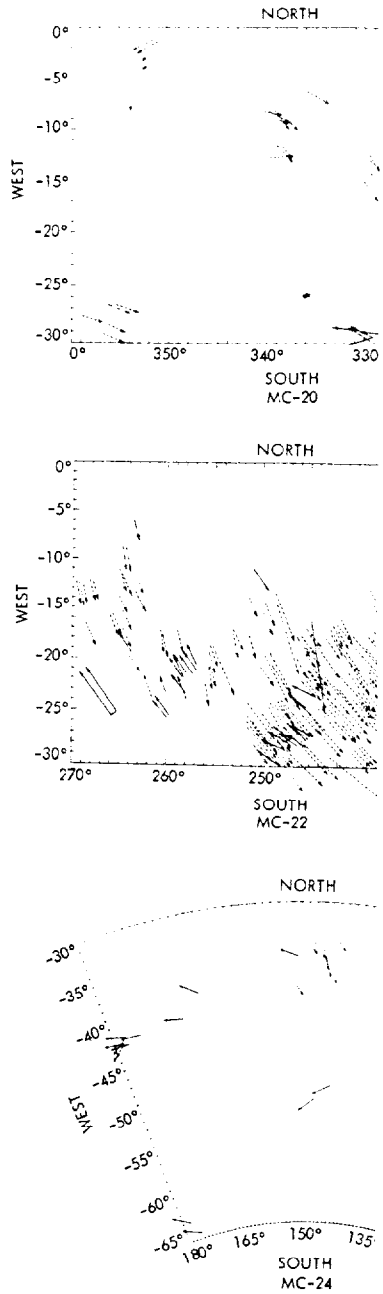

topography. There is the appearan flow away from a region center 110°W. This is the area of Tharsis region on Mars. The flow mar wind transport downhill here, alt

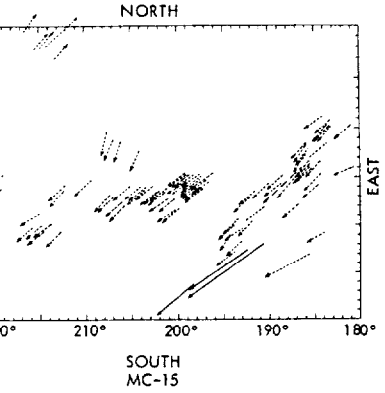

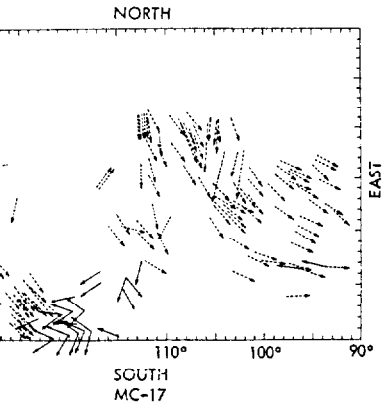

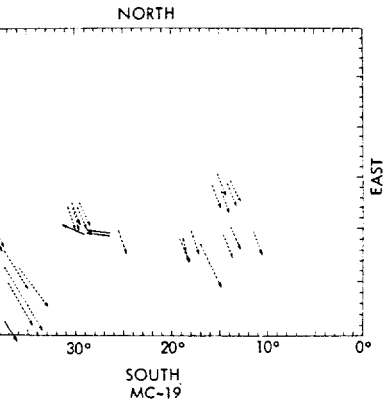

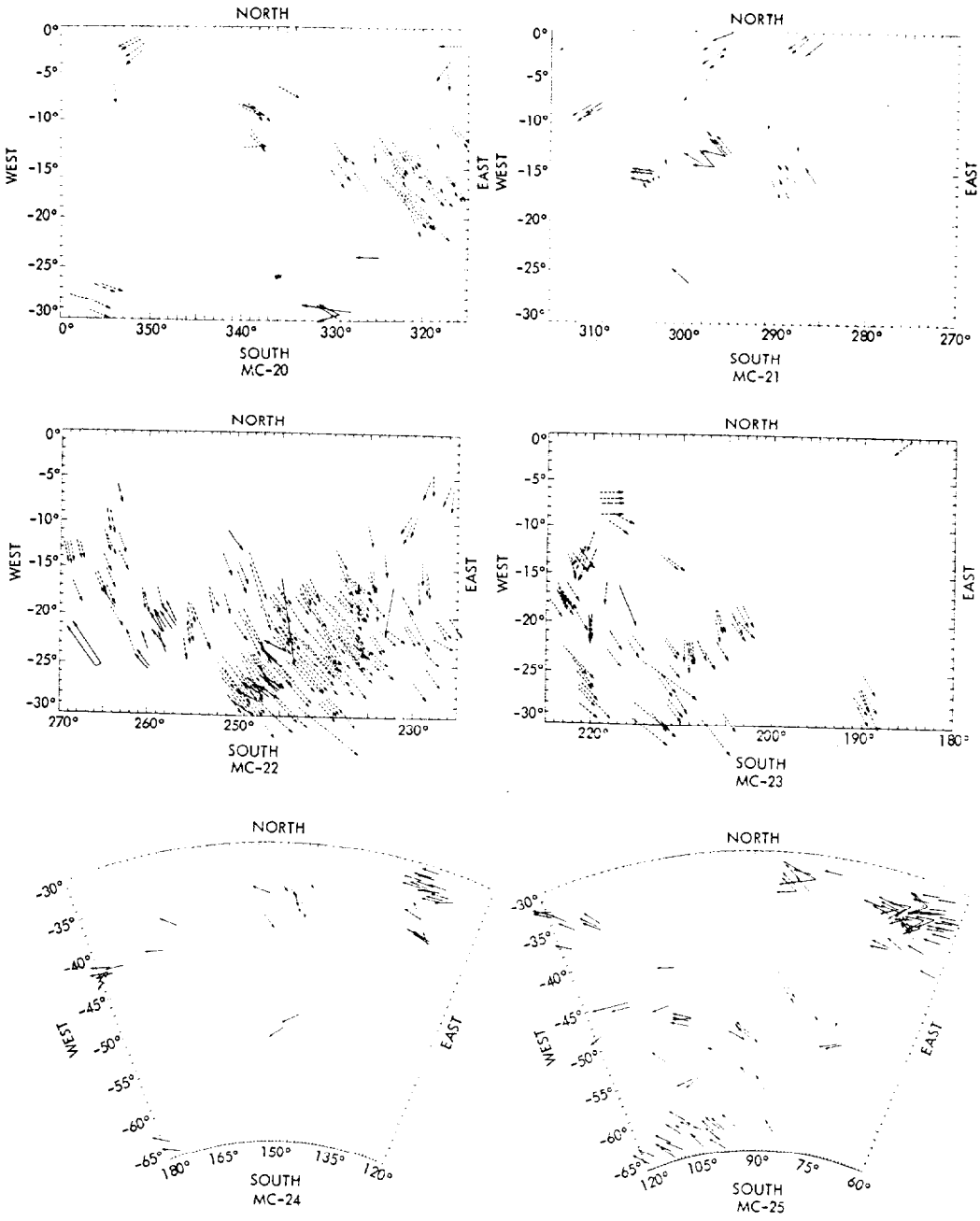

Fig. 1. (continued)

ɛation of a steady easterly flow at latitudes 20° to 40°S. This is range and initial direction of flow 1971 global dust storm, and it is this flow component is a marker

ɛuliarities may be connected with topography. There is the appearance of radial flow away from a region centered at 5°N, 110°W. This is the area of Tharsis, the highest region on Mars. The flow markers suggest wind transport downhill here, although this is not the predicted flow direction in the vicinity of such elevations in current theories during daytime. Such downhill flows are common on earth at night, however, owing to radiative cooling of the ground. A divergence or bifur-

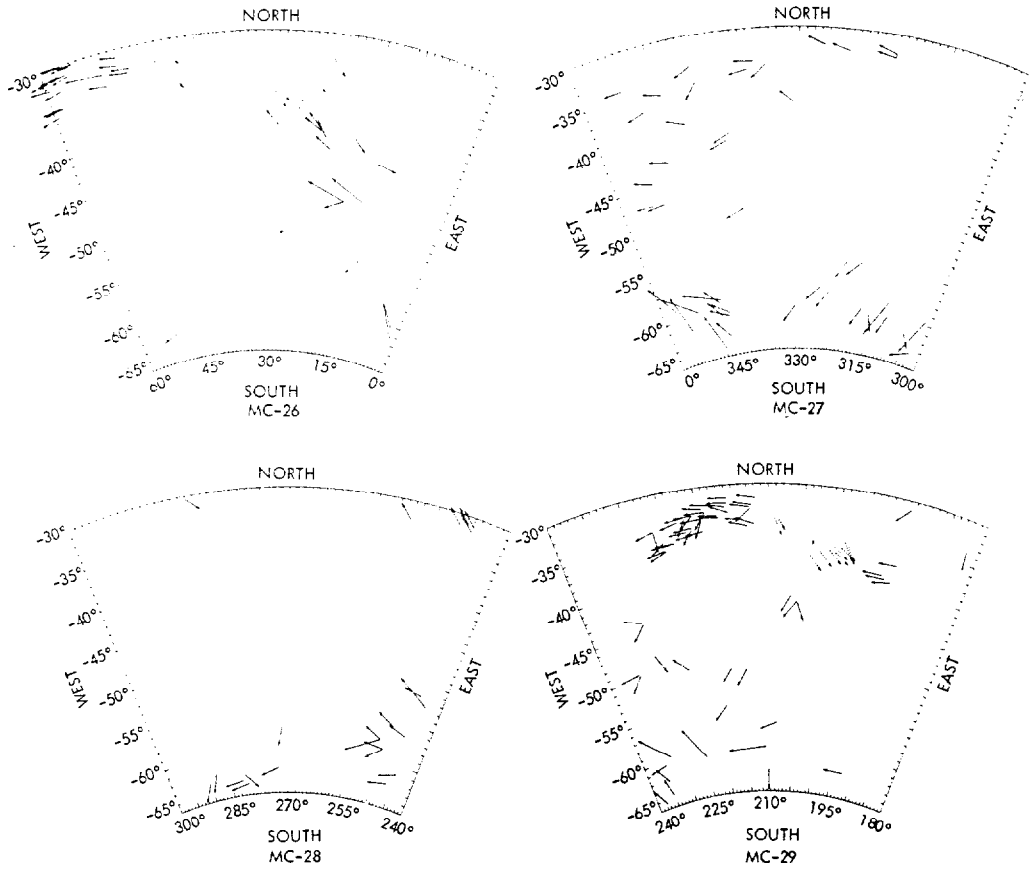

Fig. 1. (continued)

cation of the flow patterns near 20°S, 110°W, seems to be connected with the presence of rough terrain there (Figure 1*c*); the winds appear to move to avoid the rough region.

The preceding results provide us with a new estimate of the threshold velocity necessary to initiate grain motion on the Martian surface. There is a modest variation among various recent estimates of the critical velocity V above the surface boundary layer necessary to initiate grain motion on the surface. *Sagan and Pollack* [1967, 1969; see also paper 1] estimated this velocity at about 65 m/sec for a 15-mb surface pressure level, about 80 m/sec for 10 mb, and about 110 m/sec for 5 mb. *Golitsyn* [1973] proposed that these values may be reduced by about 30% by introducing sharp roughness gradients. *Hess* [1972], recalculating the problem, derives V for an 8-mb surface pressure to be between 38 and 60 m/sec, depending on the velocity distribution function through the boundary layer. Yet another independent estimate by *Gierasch and Goody* [1973] is about 30 m/sec for a surface pressure of 5 mb. The range among these models is about a factor of 2 for comparable surface pressures for the threshold velocity V_{*t} to initiate grain motion at the ground but rises to a factor of almost 4 for the velocity above the boundary layer due to differences among the models in the assumed functional form of the velocity distribution through the boundary layer. Distinguishing among these results is a matter of some importance for understanding the generation of dust storms and eolian transport on Mars. It also has a more practical importance: Lower velocities present no problem to a lander mission such as Viking, whereas the higher velocities pose grave hazards.

The existence of a 40° wide equatorial

Fig. 2. Prevailing streak direct
Lowell Observatory earth-based a
areas.

latitude band in which the streal
follow strikingly the mean general
with significant deviations outside
indicates that the global wind veloci
borders of the band are approxir
velocities appropriate for initiating g
ment on the surface. From the I

Fig. 3. Prevailing streak direction
Mari

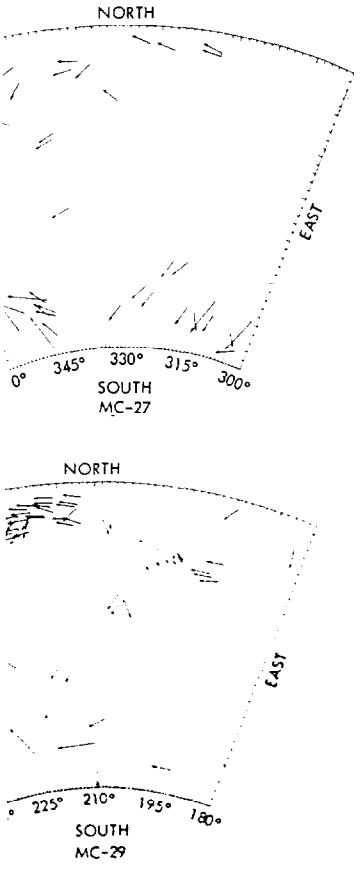

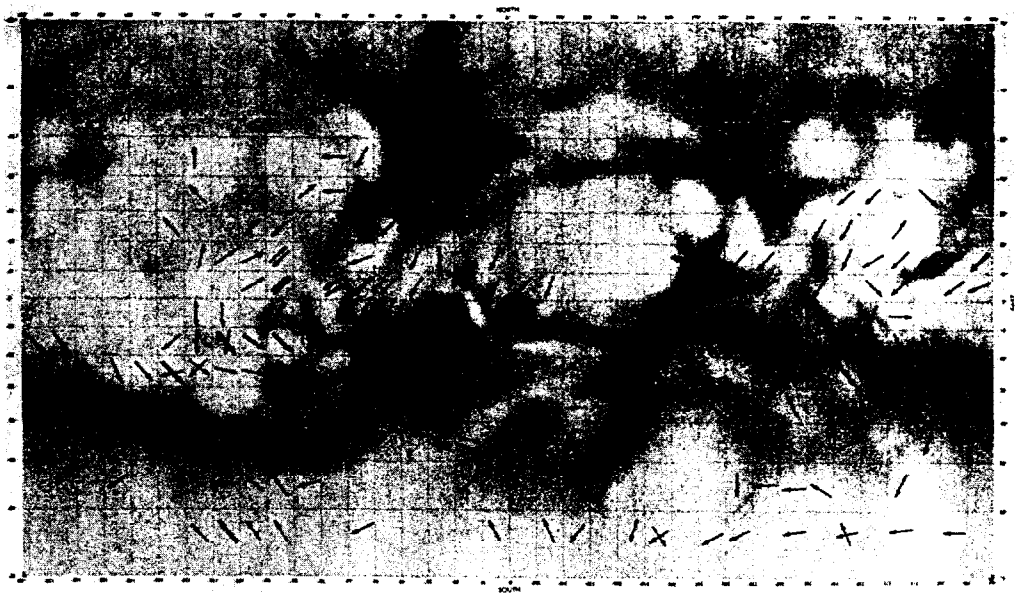

Fig. 2. Prevailing streak directions (averaged over 10° by 10° squares) superimposed on a Lowell Observatory earth-based albedo map of Mars. Thick arrows indicate heavily streaked areas.

distribution function through the
yer. Yet another independent esti-
erasch and Goody [1973] is about
r a surface pressure of 5 mb. The
; these models is about a factor of
parable surface pressures for the
locity V_{*t} to initiate grain motion
ıd but rises to a factor of almost
elocity above the boundary layer
erences among the models in the
ictional form of the velocity dis-
rough the boundary layer. Dis-
among these results is a matter
portance for understanding the
f dust storms and eolian transport
t also has a more practical im-
ower velocities present no problem
mission such as Viking, whereas
elocities pose grave hazards.
ence of a 40° wide equatorial latitude band in which the streak patterns follow strikingly the mean general circulation, with significant deviations outside this band, indicates that the global wind velocities at the borders of the band are approximately the velocities appropriate for initiating grain movement on the surface. From the Iris results (Figure 6), these velocities range from $V = 50$ to 90 m/sec above the surface boundary layer. Were topography introduced, somewhat higher velocities would be implied [*Gierasch and Sagan*, 1971]. Because grain transport typically occurs on time scales of ~10 days rather than ~1 day (this paper), it is not the mean wind of the

Fig. 3. Prevailing streak directions (averaged over 10° by 10° squares) superimposed on the Mariner 9 topographic map of Mars.

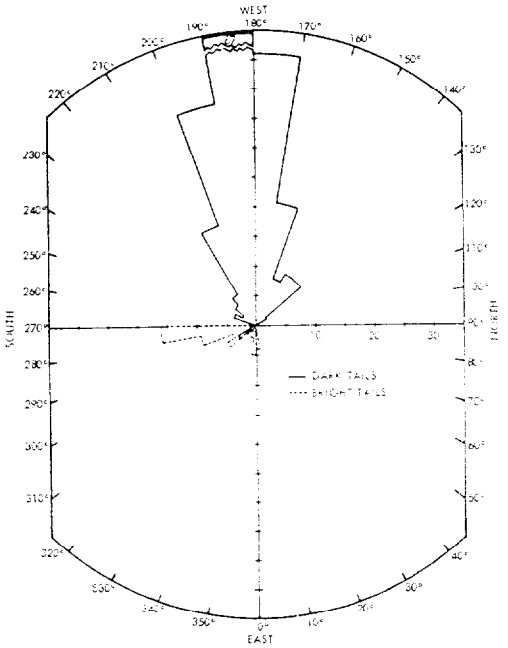

Fig. 4. Rosette diagram of the wind streaks in the Solis Lacus region shown in Figure 5. The number of dark and bright streaks is plotted as a function of azimuth.

general circulation, but the high-velocity tail of the distribution function of the general circulation winds that must be operative. These velocities lie in the middle of the range summarized above and derived from quite different considerations. Moreover, a recent revision of the wind velocities at these altitudes at the start of the dust storm, for the numerical circulation models of *Leovy and Mintz* [1969], raises these values to 40 to 60 m/sec at equatorial latitudes [*Leovy et al.*, 1973]. Velocities derived from the wavelengths of lee wave clouds [*Leovy et al.*, 1972] are of this same order.

POLAR WINDS

As we have mentioned, few wind indicators are present at very high latitudes, both because of obscuration and possibly because of efficient scouring of fine particles from the polar regions. The high splotch density in the south circumpolar region in some sense compensates for the region's low streak density: there is a marked absence of streaks in the most heavily splotched polar regions. Nevertheless, there are a few places both in the north (Mare Acidalium, MC-4) and in the south (Mare Australe, MC-25) where many streaks are directed away from the poles. This is hardly an invariable high-latitude phenomenon (there is also a westerly circumpolar component), as inspection of Figure 1 (MC-24 to MC-29) clearly shows; but it nevertheless seems noteworthy. The most straightforward explanation would be in terms of the polar cap temperature gradient winds

Fig. 5. Streak map of the Solis Lacus region of Mars superimposed on an earth-based albedo map of the area. Solid arrows represent dark streaks; dashed arrows represent bright streaks. The arrow length is appoximately four times the length of the streak. Where a number of similar streaks occur close together, only one is shown with a number to indicate how many such streaks there were. Craters with short incipient dark streaks are mapped as circles with short arrows in the direction of the incipient tail.

postulated by *Leovy et al.* [1973]. fleeing streaks in Mare Acidalium are because this mare is one of the few at these latitudes for which seasor are expected at the observed se possible that seasonal albedo variati latitudes are driven by such polar most likely mechanism would be removal of bright overlying dust, re darker material underneath, as pos several varieties of seasonal changes *Pollack*, 1967, 1969; *Sagan et al.*, 19 1].

A related phenomenon may be the collar. This dark band, surrounding ing the northern ice cap in its sumr to the pole, has been reported by m observers [e.g., *de Vaucouleurs*, 195- 1973]. Because of possible psychopl contrast effects, and especially beca interpretation of the northern moistened ground, the very exister collar has been called into question years. Mariner 9 extended mission pl

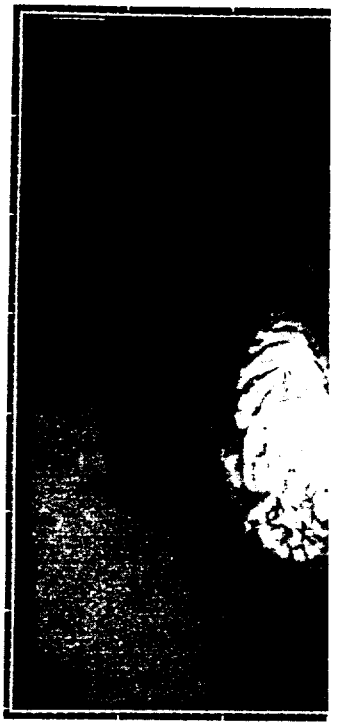

Fig. 7. The north polar cap of Ma late spring in the northe

postulated by *Leovy et al.* [1973]. The pole-fleeing streaks in Mare Acidalium are interesting because this mare is one of the few dark areas at these latitudes for which seasonal changes are expected at the observed season. It is possible that seasonal albedo variations at high latitudes are driven by such polar winds. The most likely mechanism would be the eolian removal of bright overlying dust, revealing the darker material underneath, as postulated for several varieties of seasonal changes [*Sagan and Pollack*, 1967, 1969; *Sagan et al.*, 1971; paper 1].

A related phenomenon may be the north polar collar. This dark band, surrounding and following the northern ice cap in its summer retreat to the pole, has been reported by many visual observers [e.g., *de Vaucouleurs*, 1954; *Dollfus*, 1973]. Because of possible psychophysiological contrast effects, and especially because of the interpretation of the northern collar as moistened ground, the very existence of the collar has been called into question in recent years. Mariner 9 extended mission photography has demonstrated unambiguously (Figure 7) the existence of the north polar collar. Under the circumstances, the report by earth-based visual observers that the collar follows the retreating polar cap toward the pole must now be taken seriously.

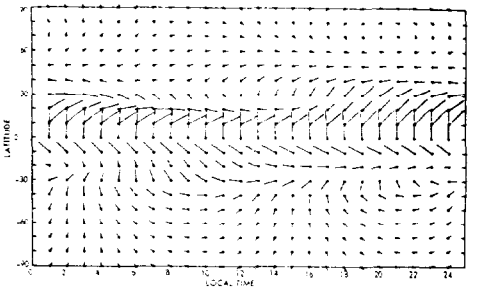

Fig. 6. Iris wind fields determined from pressure-temperature profiles of the Martian atmosphere. The season is summer in the southern hemisphere. The wind direction is into the grid points; a wind vector equal in length to one grid spacing corresponds to a velocity of 80 m/sec (courtesy of F. A. Pirraglia).

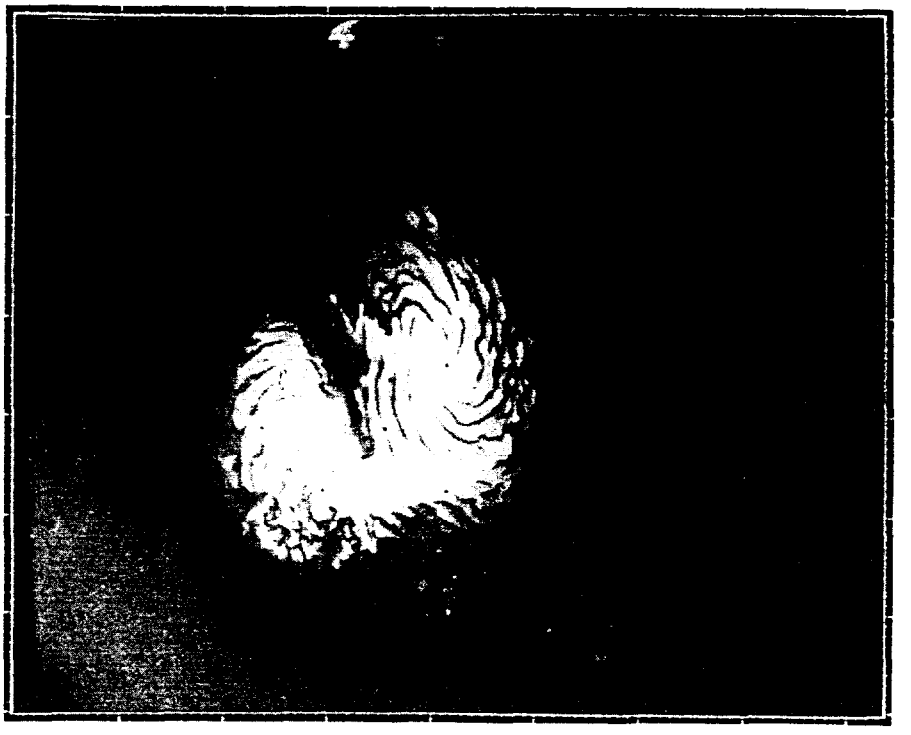

Fig. 7. The north polar cap of Mars, showing the prominent dark polar collar. The season is late spring in the northern hemisphere (MTVS 5019-40, DAS 13317550).

Both the existence of the collar and its retreat can be understood in terms of polar winds, deflating a thin, bright surface layer of dust in the immediate vicinity of the northern polar cap edge. But why did Mariner 9 find no evidence for a south polar collar? If the south collar visibility indeed follows the curve of *de Vaucouleurs* [1954, Figure 31], peak visibility corresponds to $L_s \simeq 210°$. Mariner 9 did not observe Mars near this L_s.

Another curious circumstance is that the southern circumpolar streaks are, almost without exception, dark streaks, whereas the northern streaks, and especially the Mare Acidalium streaks, are largely bright during Mariner 9 observations.

One possible explanation of some of these phenomena is the following: The steep temperature gradient between frosted and unfrosted terrains at the edge of the retreating polar ice cap produces strong winds. These winds deflate fine, bright surficial dust, uncovering the dark splotchy terrain that follows the waning periphery of the cap. The transported bright material is layered down somewhat equatorward, producing bright circumpolar streaks. High polar winds are also consistent with the probably eolian etch pits seen exclusively in polar regions.

CORRELATIONS OF STREAKS AND SPLOTCHES

We also have mapped the distribution of crater splotches over the entire Martian surface, using the techniques and cautions described above for the streak mapping program. Splotches spilling over crater ramparts and splotches unconnected with craters were not mapped. Streaks and splotches in five representative regions of Mars are displayed in Figures 8 through 12. The convention for representing streaks is described above. Splotches are represented by sketches within crater boundaries showing the approximate configurations of the splotches. Only craters

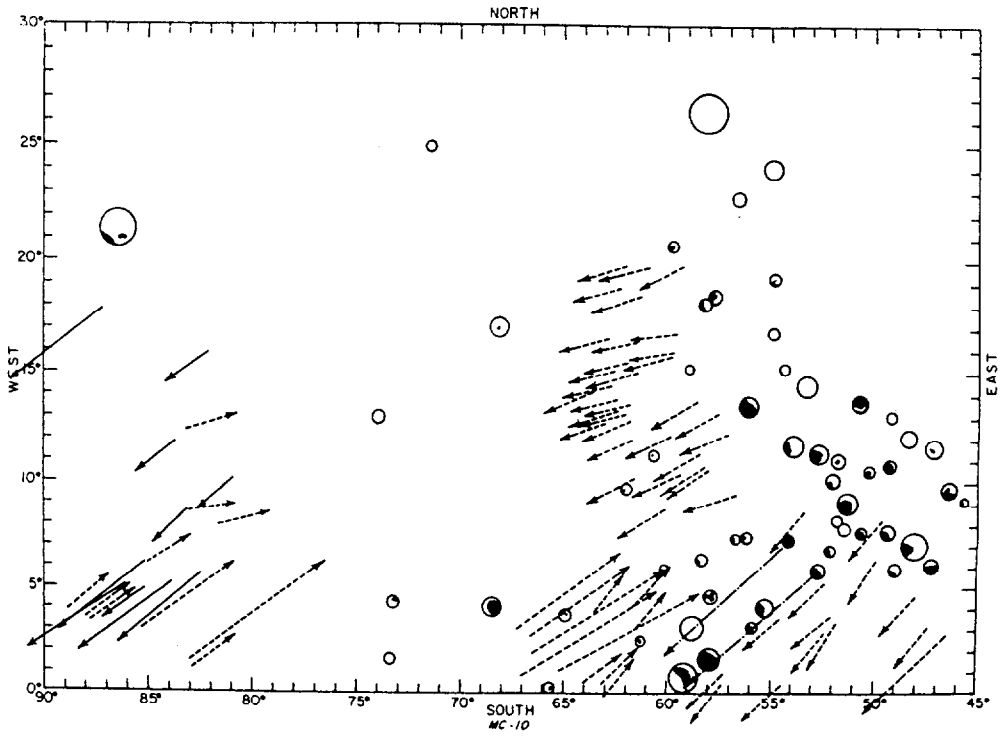

Fig. 8. Splotch-streak map of the MC-10 region. This is the area surrounding Lunae Palus. All craters larger than about 50 km in diameter and all dark crater splotches are shown. Solid arrows indicate the directions of dark crater tails; dashed arrows, bright crater tails. The arrow length is approximately four times the length of the tail. The shortest arrows shown are 2° (of latitude) and represent crater tails <60 km in length.

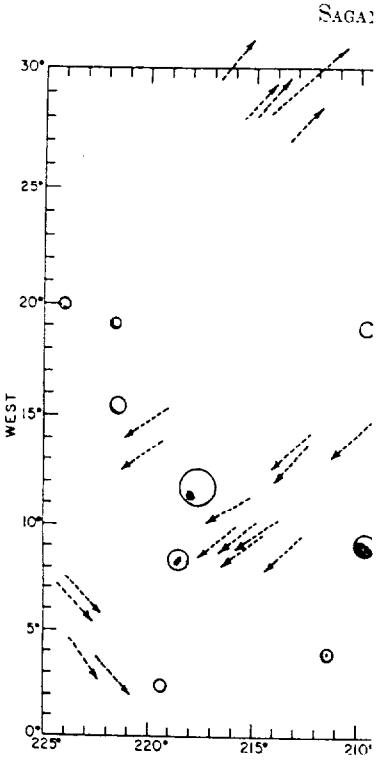

Fig. 9. Splotch-stre

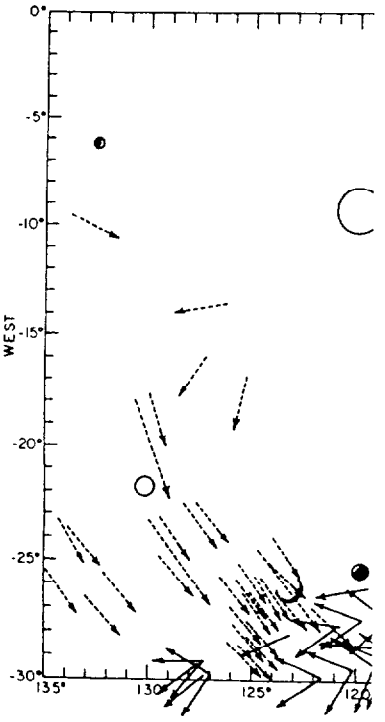

Fig. 10. Splotch-str

ION

y terrain that follows the waning
the cap. The transported bright
layered down somewhat equator-
cing bright circumpolar streaks.
winds are also consistent with the
ian etch pits seen exclusively in

ONS OF STREAKS AND SPLOTCHES

have mapped the distribution of
es over the entire Martian surface,
echniques and cautions described
the streak mapping program.
illing over crater ramparts and
connected with craters were not
eaks and splotches in five repre-
gions of Mars are displayed in
hrough 12. The convention for
streaks is described above.
e represented by sketches within
daries showing the approximate
s of the splotches. Only craters

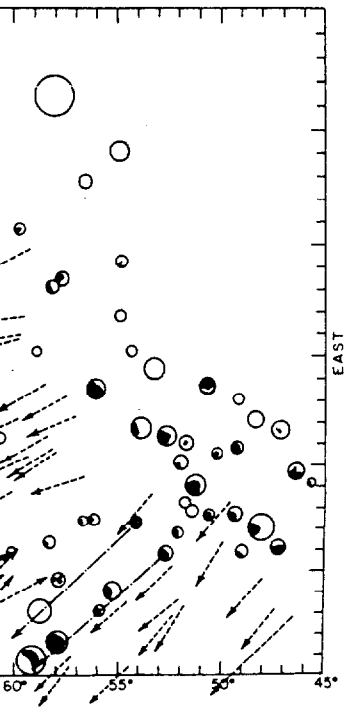

e area surrounding Lunae Palus.
rater splotches are shown. Solid
ows, bright crater tails. The ar-
. The shortest arrows shown are

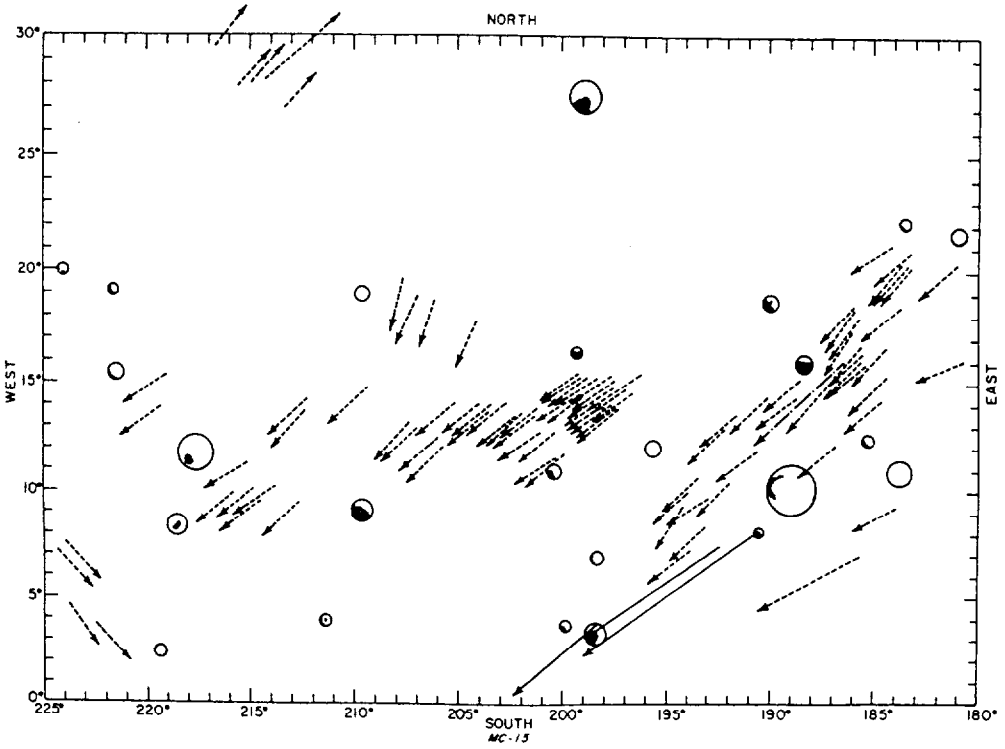

Fig. 9. Splotch-streak map of the MC-15 region Cerberus-Elysium.

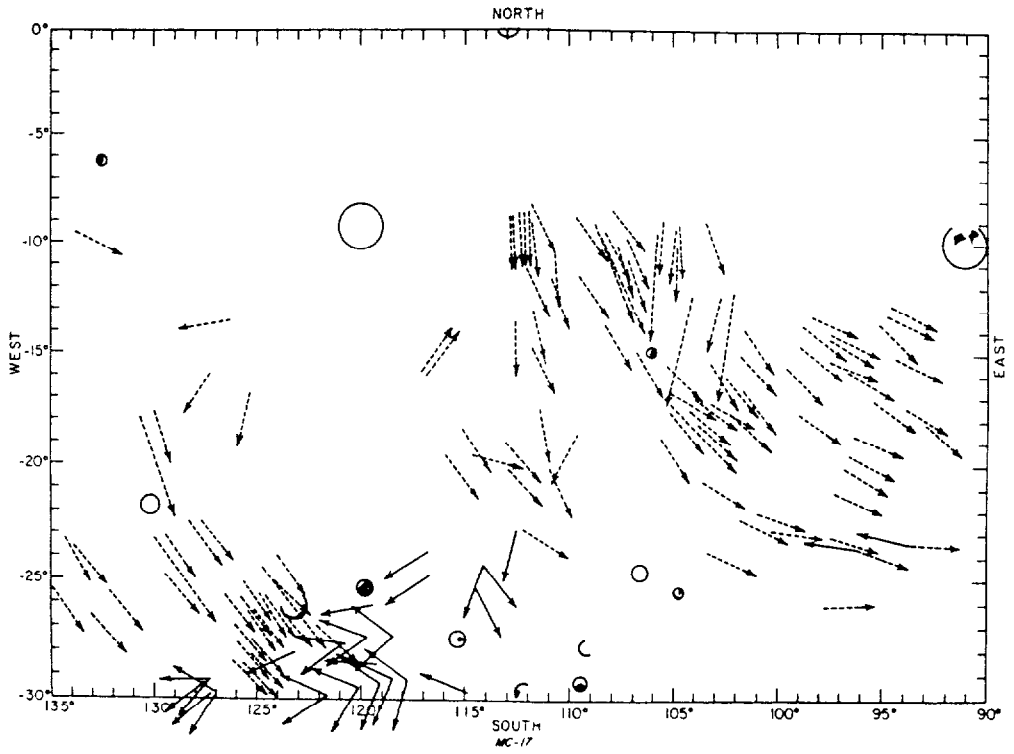

Fig. 10. Splotch-streak map of the MC-17 region Tharsis-Daedelia.

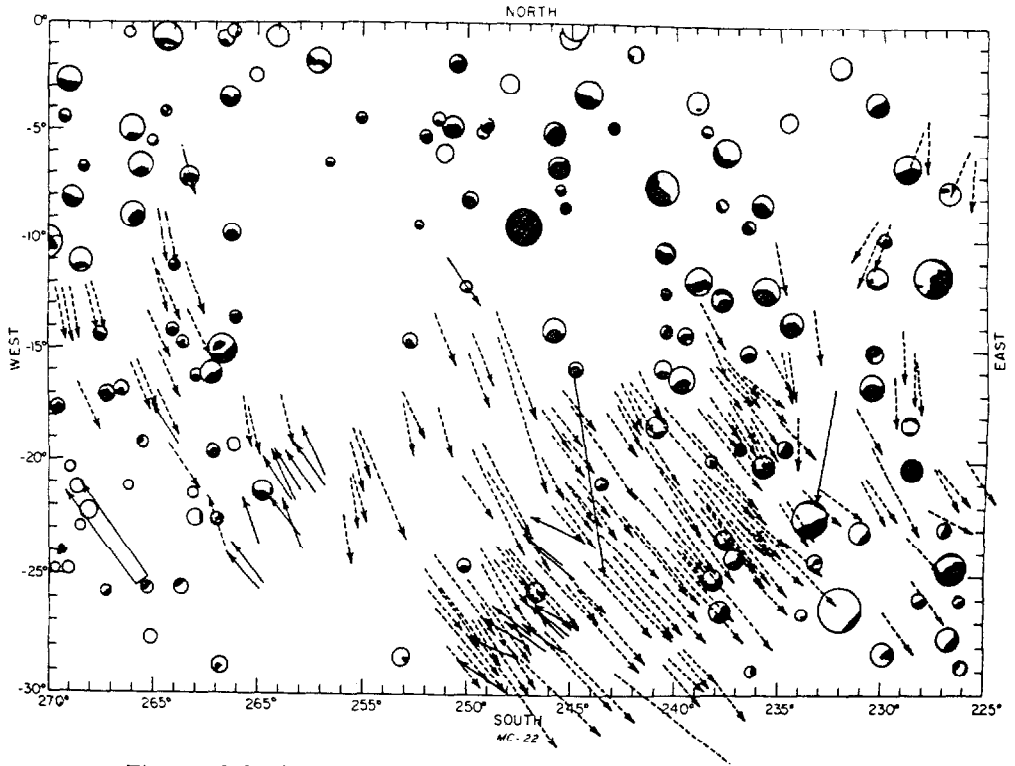

Fig. 11. Splotch-streak map of the MC-22 region Mare Tyrrhenum-Hesperia.

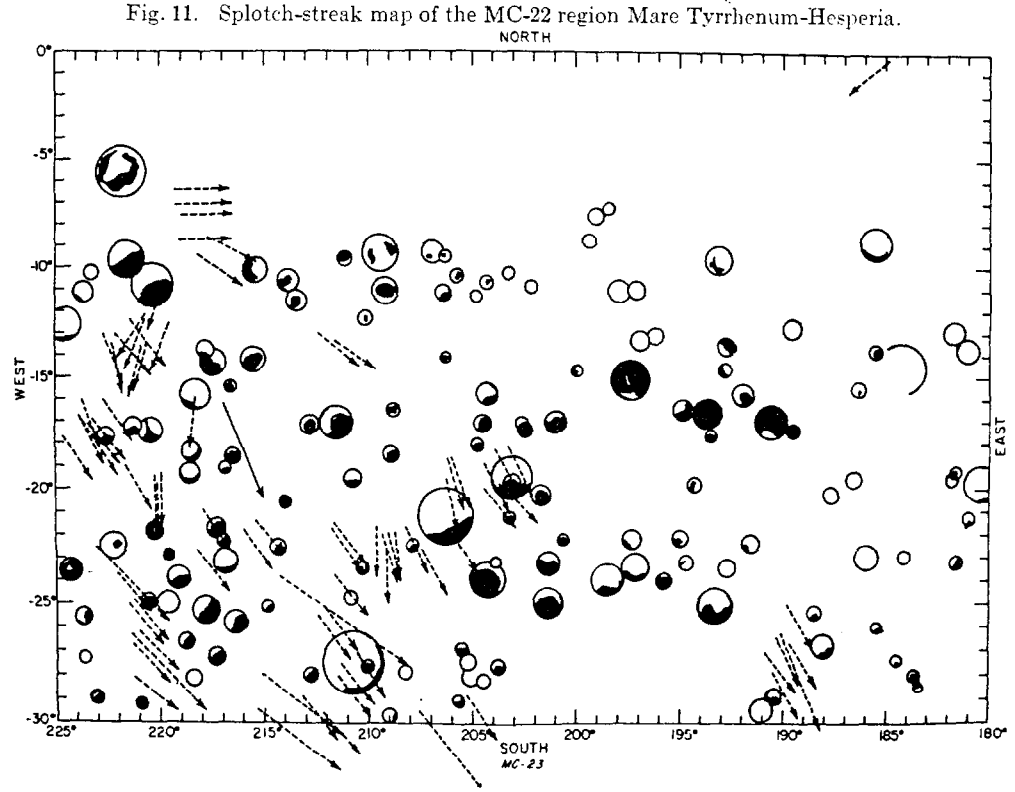

Fig. 12. Splotch-streak map of the MC-23 region Mare Cimmerium-Zephyria.

larger than about 50 km are sho
that splotches tend to be localized
face of the containing crater (cf.
There is, at least in many cases,
for splotches in adjacent craters to
in the same face of their respect
This face tends to be the direct
which the wind has been blowing, a
the predominant nearby streak wir
indicators.

As is usual in our present ignorance
surface processes, there are two e
of this correlation, each the obve
other. In the first view, the winds
dark material into the craters, wl
accumulated against the leeward ra
the second view, the winds have pi
deflated bright material off the leewai
of the craters, exposing the underly
material, possibly basement rock. Tl
streaks would then bear a closer
to Saharan sand streamers, describe
[1963] as 'relatively thin, ribbon- or
accumulations of sand downwind fro
source areas or from topographic ec
Where long, straight, parallel and
by relatively sand-free strips, the
indicate consistency and direction
moving winds.'

Accordingly, we postulate some
Mars in which dark mobile mate
crater floors is overlain with bri
material, perhaps as a consequen
or global dust storms. Subsequent
the crater produces long, bright
streaks emanating from the crater, a
ally exposes underlying dark mate
interior leeward side of the crater.
winds, possibly from another dire
can deflate the exposed dark material
incipient dark tails. Dark splot
associated dark tails are known, e.g., i
[paper 1, Figure 27]. The developm
crater tails from craters with pre-exi
tails is also known, e.g., in Hesperia
Figure 23]. These views are cons
the conclusions that we will dra
detailed study of albedo variation
selected regions, Syrtis Major, Lu
and Promethei Sinus. In other case
splotchy material may be bedroc
dark streaks may be produced by
overlying bright material.

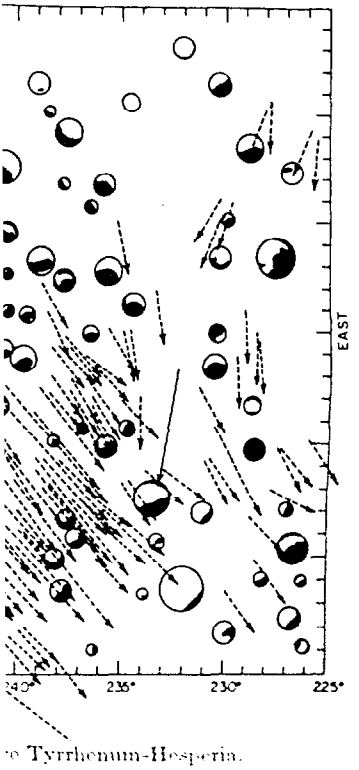

e Tyrrhenum-Hesperia.

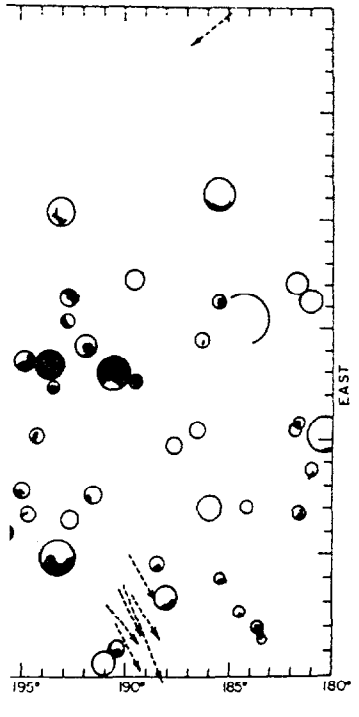

e Cimmerium-Zephyria.

larger than about 50 km are shown. We see that splotches tend to be localized toward one face of the containing crater (cf. paper 1). There is, at least in many cases, a tendency for splotches in adjacent craters to be localized in the same face of their respective craters. This face tends to be the direction toward which the wind has been blowing, according to the predominant nearby streak wind direction indicators.

As is usual in our present ignorance of Martian surface processes, there are two explanations of this correlation, each the obverse of the other. In the first view, the winds have blown dark material into the craters, where it has accumulated against the leeward ramparts. In the second view, the winds have preferentially deflated bright material off the leeward ramparts of the craters, exposing the underlying darker material, possibly basement rock. The resulting streaks would then bear a closer relationship to Saharan sand streamers, described by *Smith* [1963] as 'relatively thin, ribbon- or banner-like accumulations of sand downwind from localized source areas or from topographic constrictions. Where long, straight, parallel and separated by relatively sand-free strips, they serve to indicate consistency and direction of sand-moving winds.'

Accordingly, we postulate some cases on Mars in which dark mobile material within crater floors is overlain with bright mobile material, perhaps as a consequence of local or global dust storms. Subsequent deflation of the crater produces long, bright downwind streaks emanating from the crater, and eventually exposes underlying dark material on the interior leeward side of the crater. Subsequent winds, possibly from another direction, then can deflate the exposed dark material, producing incipient dark tails. Dark splotches with associated dark tails are known, e.g., in Bosporus [paper 1, Figure 27]. The development of dark crater tails from craters with pre-existing bright tails is also known, e.g., in Hesperia [paper 1, Figure 23]. These views are consistent with the conclusions that we will draw from a detailed study of albedo variations in three selected regions, Syrtis Major, Lunae Palus, and Promethei Sinus. In other cases, the dark splotchy material may be bedrock, and the dark streaks may be produced by deflation of overlying bright material.

Syrtis Major

At Mariner 9 resolution, the classical albedo feature Syrtis Major is outlined by a concentration of bright and dark streaks. The bright streaks dominate near the western (stable) edge of Syrtis Major. The dark streaks outline the eastern, variable edge (Figure 13) of Syrtis Major (paper 1). Telescopic evidence suggests that the eastern boundary of Syrtis Major varies seasonally [*Antoniadi*, 1930].

Since the end of the 1971 dust storm, Mariner 9 photography has revealed a gradual darkening of Syrtis Major at resolutions of the wide-angle camera (Figures 14 to 16) and the narrow-angle camera (Figures 17 to 20). This darkening resulted largely from the appearance, development, and merging of dark crater tails of the type seen in Figure 19, which are characteristic of Syrtis Major. In other areas, dark tails do not have the patchy, discontinuous appearance of the Syrtis Major tails. This nonuniform patchiness of the tails and their tendency to shed tangentially from topographic protuberances such as crater walls suggest that they are produced by eolian erosion of extensive, but very thin, deposits of bright material, resulting in the exposure of dark, wind-resistant, underlying material. Radar evidence suggests that the region of Figure 13 is a relatively smooth surface, sloping from west to east (left to right on Figure 13), making it a likely locale for eolian transport.

We assume that, after the 1971 dust storm, much of this slope was covered by a thin layer of bright dust. Subsequent winds, blowing predominantly downslope, have scoured off this material, especially in regions where wind speeds are intensified by topography. A close examination of the high-resolution narrow-angle pictures (Figures 17 to 20) is especially instructive in this context. Many instances of dark tails or sections of dark tails shedding off craters can be seen. This is especially evident in Figure 20.

We postulate efficient microtraps for the dust scoured off in the above manner. Our model predicts that Syrtis Major will continue to darken until it is affected by either a local or global dust storm. The contrasts involved between the dark and bright portions of Syrtis Major are small, being typically about 10% (for the albedo markings in Figure 18).

Fig. 13. General view of Syrtis Major. This wide-angle picture, centered at 13°N, 283°W, is about 360 km across (MTVS 4186-72, DAS 07147383).

As in other regions of Mars, white streaks exist in Syrtis Major but have not been seen to change (Figure 21). Their nature (erosional or depositional) and time of origin (before, during, or after the dust storm) remain enigmatic.

LUNAE PALUS

Another region studied lies close to the classical albedo feature Lunae Palus, suspected of being both a seasonal and secular variable by telescopic observers [*Focas*, 1961]. Mariner 9 photography resolves the region into a wide, deep channel dissecting relatively smooth surrounding plains (Figure 22).

Although no albedo changes in these plains have yet been detected in Mariner 9 pictures, strong localized albedo changes have been found within the channel itself (Figure 23). At least three separate areas were seen to darken during the mission. The largest of these is about 20 by 70 km in size. Only a slight change is evident at wide-angle camera resolution between revolutions 125 and 160, but a very pronounced darkening occurred sometime during the 39-day interval between revolutions 160 and 238 (Figure 23).

A high-resolution view of the floor of the channel, including a section of the largest of the three darkening areas, is shown in Figure 24. This area is outlined in Figure 22. At the resolution of the narrow-angle camera, it is clear that darkening occurred within the channel between revolutions 125 and 160 (Figure 25), although this is not evident at wide-angle camera resolution (Figure 23). The two views shown in Figure 25 do not overlap exactly and are not aligned with respect to each other. They are therefore difficult to compare directly. To facilitate the comparison, three arrows are shown in each view. The top two point to a pair of dark, round spots; the bottom arrow points to a characteristic bend in the small

channel seen in the figure. The view (was obtained on revolution 125; th right, 17 days later on revolution change that has occurred in this regic evident in Figure 26, which shows scaled, similarly projected, and alig of the region surrounding the three Figure 25. The two dark round spc 1 km) can be seen just below the cer

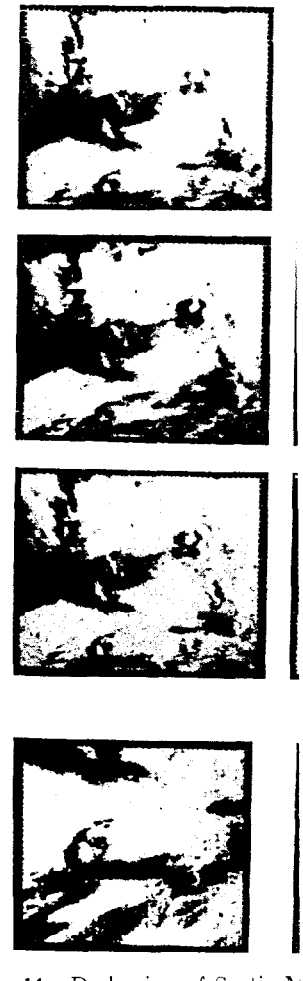

Fig. 14. Darkening of Syrtis M three rows is about 270 km acro proximately to the upper half of tion 233. Stanford picture differen to right): revolution 233, revolutic revolution 155, revolution 430, rev 0191, 102105-6-7). The last row sh Left to right: revolution 155, r 283.9°W; width = 140 km (Stanf photometric geometry is closely si on revolution 430.

ON

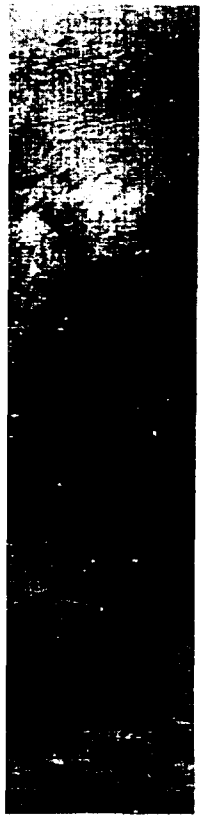

ure, centered at 13°N, 283°W,
3 07147383).

camera resolution between revo-
nd 160, but a very pronounced
urred sometime during the 39-day
veen revolutions 160 and 238

olution view of the floor of the
ding a section of the largest of the
ng areas, is shown in Figure 24.
outlined in Figure 22. At the
the narrow-angle camera, it is
kening occurred within the channel
utions 125 and 160 (Figure 25),
s not evident at wide-angle camera
igure 23). The two views shown
lo not overlap exactly and are not
respect to each other. They are
ficult to compare directly. To
comparison, three arrows are
h view. The top two point to a
round spots; the bottom arrow
characteristic bend in the small

channel seen in the figure. The view on the left was obtained on revolution 125; that on the right, 17 days later on revolution 160. The change that has occurred in this region is made evident in Figure 26, which shows rectified, scaled, similarly projected, and aligned views of the region surrounding the three arrows in Figure 25. The two dark round spots (about 1 km) can be seen just below the center of the window in the left (revolution 125) and middle (revolution 160) sections of Figure 26. Similarly the characteristic bend in the channel occurs at the bottom left corner of both sections. The right section of Figure 26 shows a picture-element by picture-element difference of the two sections on the left. Notice that the two round spots cannot be seen in the difference, as they have not changed. Similarly the channel

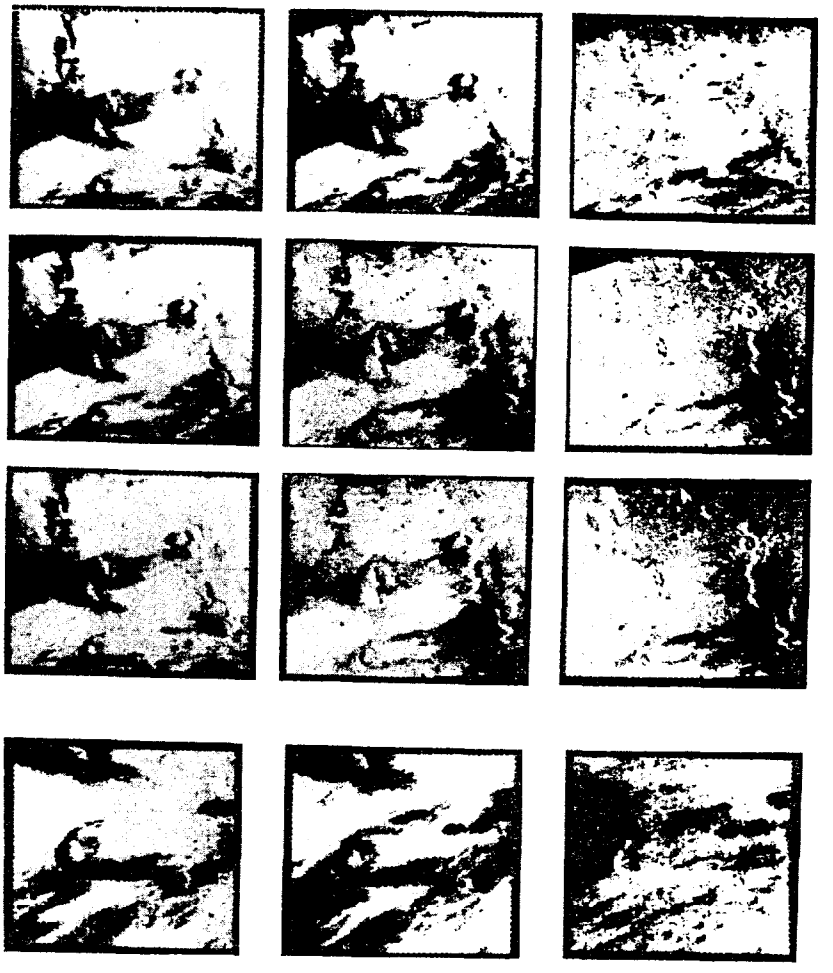

Fig. 14. Darkening of Syrtis Major at wide-angle resolutions. The area shown in the top three rows is about 270 km across and is centered at 15.2°N, 282.8°W. It corresponds approximately to the upper half of Figure 13. First row (left to right): revolution 155, revolution 233, Stanford picture difference: revolution 233 minus revolution 155. Second row (left to right): revolution 233, revolution 430, revolutions 430 minus 233. Third row (left to right): *revolution 155, revolution 430, revolutions 430 minus 155* (*Stanford AIL Picture Product* STN 0191, 102105-6-7). The last row shows a closeup of the bottom sections of the window above. Left to right: revolution 155, revolution 233, revolutions 233 minus 155. Center 13.8°N, 283.9°W; width = 140 km (Stanford AIL Picture Product STN 0164, 041505). Note that the photometric geometry is closely similar on revolutions 155 and 233, but significantly different on revolution 430.

Fig. 15. Darkening of Syrtis Major at wide-angle camera resolution. The area shown is about 140 km across and is centered at 11.7°N, 284.5°W. It corresponds to the lower left of Figure 13. Left to right: revolution 155, revolution 233, revolutions 233 minus 155 (Stanford AIL Picture Product STN 0164, 041506).

Fig. 16. Darkening of Syrtis Major at wide-angle camera resolution. The area shown is about 250 km across and is centered at 14.6°N and 282.8°W. It corresponds to the upper half of Figure 13. Left to right: revolution 155, revolution 430, revolutions 430 minus 155. Because the photometric geometry differs appreciably between revolutions 155 and 430, topographic detail has not been cancelled successfully in the picture difference (Stanford AIL Picture Product STN 0191, 102101).

Fig. 17. Darkening of Syrtis Major at narrow-angle camera resolution. The area shown is about 50 km across and is centered at 13.2°N and 282.9°W. Left to right: revolution 233, revolution 430, revolutions 430 minus 233. The photometric geometry differs considerably between the two views, and topographic detail remains in the picture difference (e.g., the crater at lower right) (Stanford AIL Picture Product STN 0191, 102111).

is not evident. However, a significant amount of darkening is seen to have taken place in the immediate neighborhood of the two dark spots between revolutions 125 and 160. The lateral extent of the change can be inferred from the fact that the two spots are about 10 km apart.

The observed darkening of regions within the Lunae Palus channel can best be understood in terms of the gradual removal, by winds, of fine bright dust deposited during the 1971 dust storm over the albedo markings within the channel (Figures 24, 25, 26). It is possible that a channeling and intensification of winds may be produced by the main Lunae Palus channel, thus leading to more effective eolian erosion within the channel than on the surrounding plains. This would result in a greater apparent variability (e.g., darkening) within

Fig. 18. Another example of tl
lution. The area shown is about
row (left to right): revolution 155,
to right): revolutions 233 and 4
factory alignment could not be
geometry between the two pict

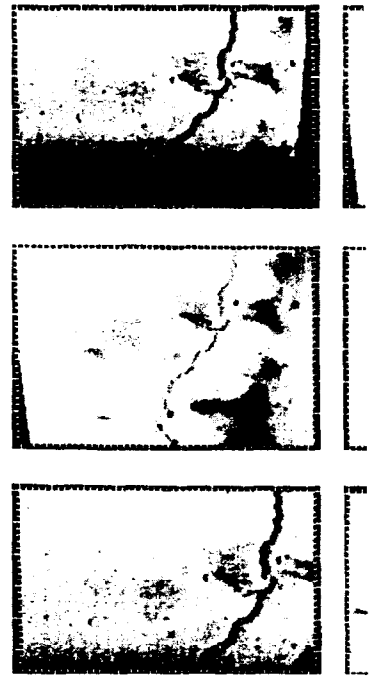

Fig. 19. Appearance and devel
camera resolution. Top row shows a
Left to right: revolution 155, rev
geometry is similar in the two vie
middle row shows an enlargement
across). Left to right: revolution 1
row shows a corresponding enlarg
(Stanford AIL Picture Product STN

resolution. The area shown is
corresponds to the lower left of
lutions 233 minus 155 (Stanford

resolution. The area shown is
It corresponds to the upper half
olutions 430 minus 155. Because
utions 155 and 430, topographic
ifference (Stanford AIL Picture

era resolution. The area shown
V. Left to right: revolution 233,
e geometry differs considerably
the picture difference (e.g., the
. 102111).

dust deposited during the 1971
over the albedo markings within
(Figures 24, 25, 26). It is possible
neling and intensification of winds
duced by the main Lunae Palus
s leading to more effective eolian
n the channel than on the surround-
This would result in a greater
riability (e.g., darkening) within

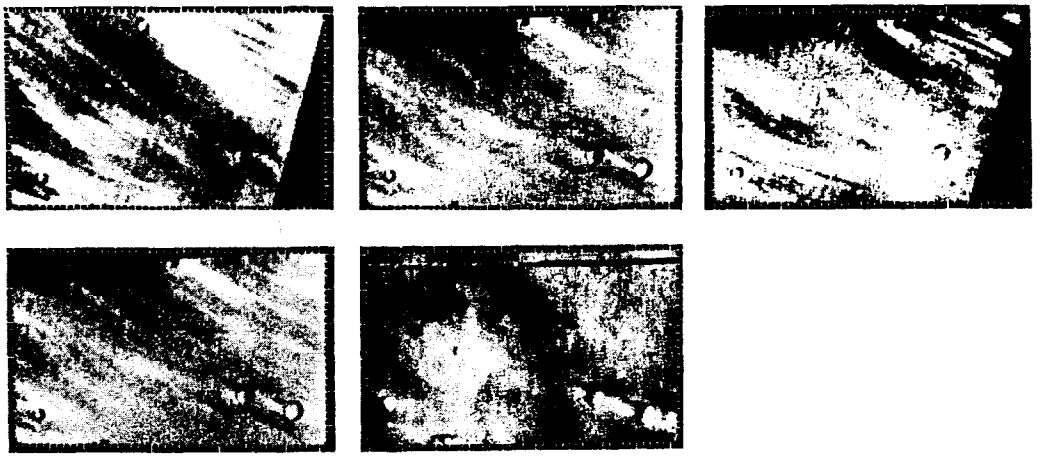

Fig. 18. Another example of the darkening of Syrtis Major at narrow-angle camera resolution. The area shown is about 50 km across and is centered at 10.8°N and 283.6°W. Top row (left to right): revolution 155, revolution 233, revolutions 233 minus 155. Bottom row (left to right): revolutions 233 and 430. These two pictures were not differenced because satisfactory alignment could not be obtained owing to a significant change in the photometric geometry between the two pictures (Stanford AIL Picture Product STN 0191, 102113).

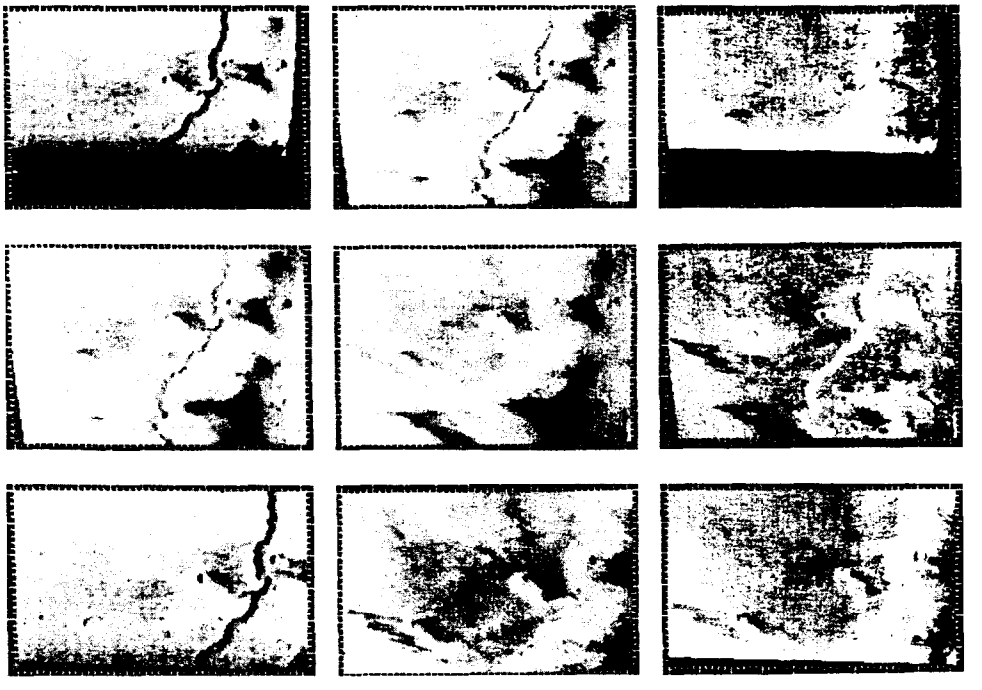

Fig. 19. Appearance and development of dark tails in Syrtis Major at narrow-angle camera resolution. Top row shows an area about 44 km across centered at 14.9°N and 281.6°W. Left to right: revolution 155, revolution 237, revolutions 237 minus 155. The photometric geometry is similar in the two views (Stanford AIL Picture Product STN 0172, 040604). The middle row shows an enlargement of the center section of the above region (about 22 km across). Left to right: revolution 155, revolution 237, revolutions 237 minus 155. The bottom row shows a corresponding enlargement of the lower left corner of the original window (Stanford AIL Picture Product STN 0172, 06065-6).

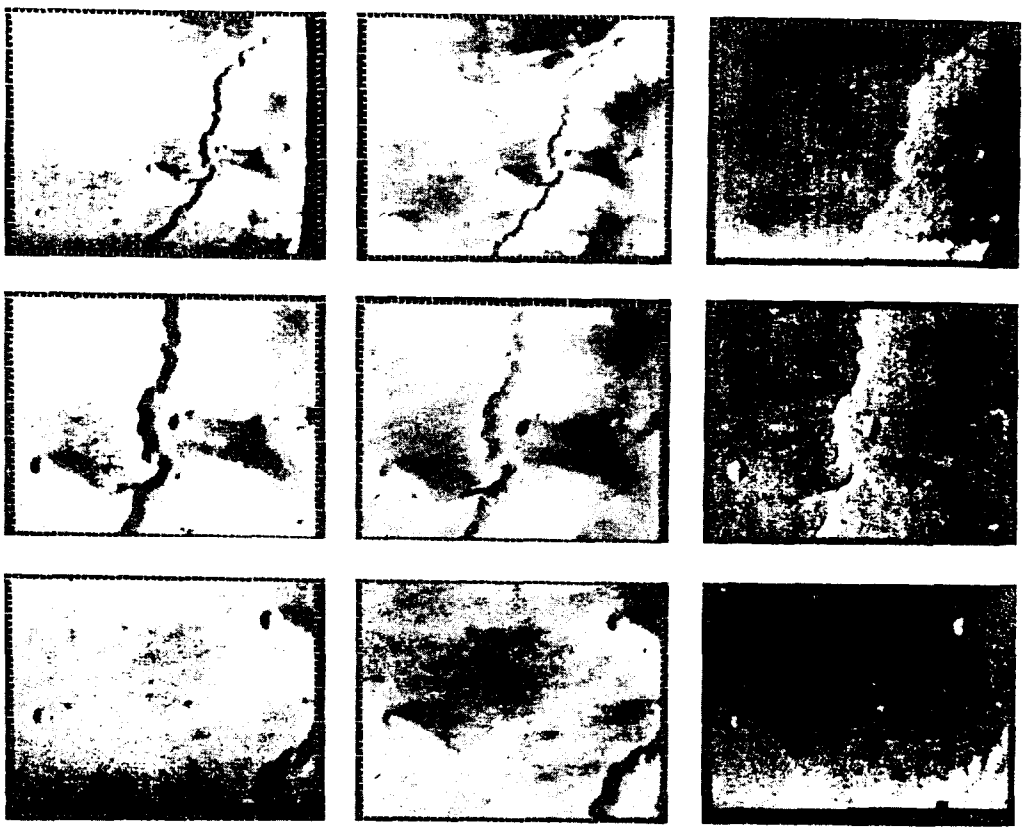

Fig. 20. Development of dark tails at narrow-angle camera resolution in the region of Figure 19. Top row (left to right): revolution 155, revolution 233, revolutions 233 minus 155. Middle row: revolution 237, revolution 430, revolutions 430 minus 237. Bottom row: revolution 155, revolution 430, revolutions 430 minus 155. The photometric geometry is similar for revolutions 155 and 233, but differs significantly for revolution 430. The area is about 50 km across and is centered at 14.9°N, 281.9°W (Stanford AIL Picture Products STN 0191, 102114, 102115, 102116, 102117).

Fig. 21. Permanence of white streaks in Syrtis Major at narrow-angle camera resolution. The area is about 35 km and is centered at 4.6°N, 294°W. Left to right: revolution 194, revolution 233, revolutions 233 minus 194. The photometric geometry differs in the two views, making it impossible to cancel topographic features in the picture difference (Stanford AIL Picture Products STN 0191, 102110).

Fig. 22. Overall wide-angle cam
The picture is about 300 km acr
Figure 24 (JPL Roll 1329, 181918).

the channel than on the plains after
dust storm. Likewise, the great Cop
valley, so long that one end may
noon when the other is before sun
generate and channel very high win

Fig. 23. Changes within the L
Left to right: revolutions 125, 160,
nel during the 39-day interval bet
width = 260 km (Stanford AIL Pi

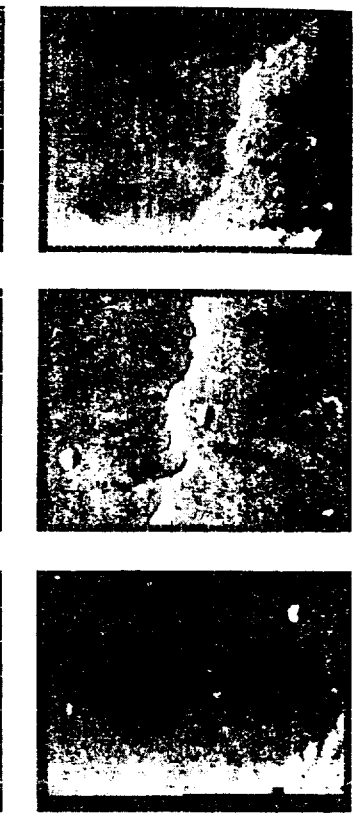

era resolution in the region of
233, revolutions 233 minus 155.
nus 237. Bottom row: revolution
metric geometry is similar for
n 430. The area is about 50 km
ure Products STN 0191, 102114.

narrow-angle camera resolution.
ft to right: revolution 194, rev-
metry differs in the two views.
icture difference (Stanford AIL

Fig. 22. Overall wide-angle camera view of Lunae Palus, centered at about 21°N, 63°W. The picture is about 300 km across. The region outlined is shown at high resolution in Figure 24 (IPL Roll 1329, 181918).

the channel than on the plains after a major dust storm. Likewise, the great Coprates rift valley, so long that one end may be near noon when the other is before sunrise, may generate and channel very high winds.

Promethei Sinus

Figure 27 is a wide-angle view of Promethei Sinus, an extensively splotched, cratered region near the south pole of Mars. According to

Fig. 23. Changes within the Lunae Palus channel at a wide-angle camera resolution. Left to right: revolutions 125, 160, and 238. Note the pronounced darkening within the channel during the 39-day interval between revolutions 160 and 238. Centered at 23°N, 66°W; width = 260 km (Stanford AIL Picture Products STN 0166, 042911, 042912).

Fig. 24. Narrow-angle camera view of the region outlined in Figure 22. Revolution 160. Centered at 22°N, 65°W; width = 75 km (IPL 1329, 185802).

Antoniadi [1930], Promethei Sinus is variable, but it is not known whether the variations are seasonal. For the study of variable features, the two regions outlined in Figure 27 are of special interest. The more important of the two is shown at high resolution in Figure 28. Two kinds of characteristic dark splotches are seen: (1) those inside craters, usually running up against the crater's inner walls, and (2) splotches lying outside of craters. The latter have a very characteristic morphology, one long edge being rather amorphous in outline and the other scalloped and pointed.

Dark splotches tend to lie on the downwind side of craters. On this basis, the prevalent wind direction in Figure 28 is from top to bottom. Scalloped edges are also characteristic of eolian phenomena, the wind always blowing at right angles to the scalloped edge. Thus one inference from the scallops is a wind direction from top to bottom in Figure 28, which would be consistent with that inferred from the location of splotches within the two craters. In this case, the dark scalloped splotches could be interpreted as underlying, wind-resistant dark material, exposed by scouring off bright overlying material. Other interpretations are discussed in the next section. The contrast between the bright and dark splotches in this region is about 20%.

Several regions of special interest are designated by letters in Figure 28; their behavior during the Mariner 9 mission is documented in Figures 29 to 34. Figure 29 shows the development in less than 13 days (i.e., sometime between revolutions 99 and 126) of a 10-km dark region. This region, resembling a leaf or a spearhead, subsequently remained unchanged, even though surrounding areas were undergoing variation.

Fig. 25. Right: revolution 160 projection. Left: Same region, s exactly and are not aligned with point to a pair of dark spots, an small channel (IPL Roll 1329, 1242(

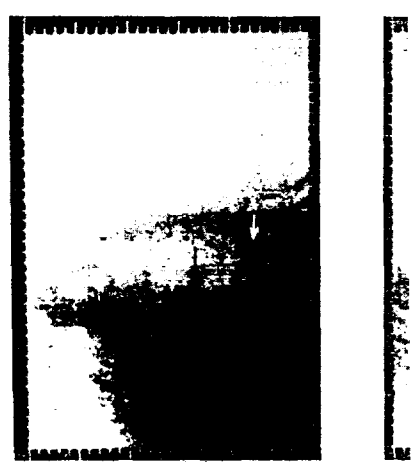

Fig. 26. Region of the two da revolution 125. Middle: revolutio aligned relative to each other and picture difference at right. Note th at 22.6°N, 64.5°W; width = 30 k

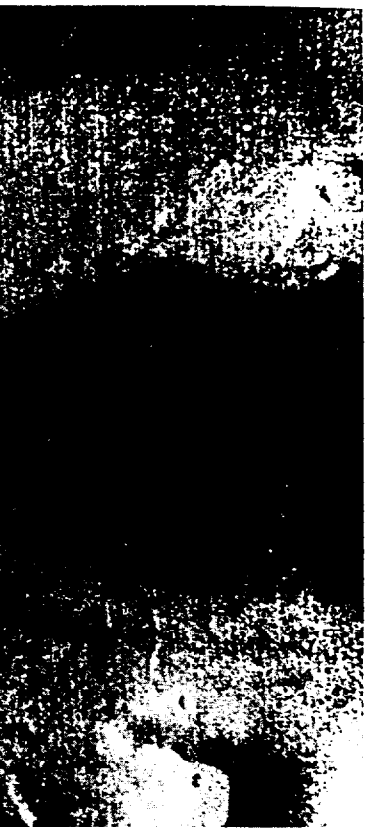

. in Figure 22. Revolution 160.
L 1329, 185802).

bottom in Figure 28, which would
nt with that inferred from the
splotches within the two craters. In
e dark scalloped splotches could be
as underlying, wind-resistant dark
posed by scouring off bright over-
ial. Other interpretations are dis-
e next section. The contrast between
nd dark splotches in this region is

gions of special interest are desig-
tters in Figure 28; their behavior
Mariner 9 mission is documented
29 to 34. Figure 29 shows the
in less than 13 days (i.e., sometime
olutions 99 and 126) of a 10-km
This region, resembling a leaf or
subsequently remained unchanged,
surrounding areas were undergoing

Fig. 25. Right: revolution 160. Same area as in Figure 24, but shown in orthographic projection. Left: Same region, seen on revolution 125. These two views do not overlap exactly and are not aligned with respect to each other. In each view, the upper two arrows point to a pair of dark spots, and the bottom arrow points to a characteristic bend in the small channel (IPL Roll 1329, 124209).

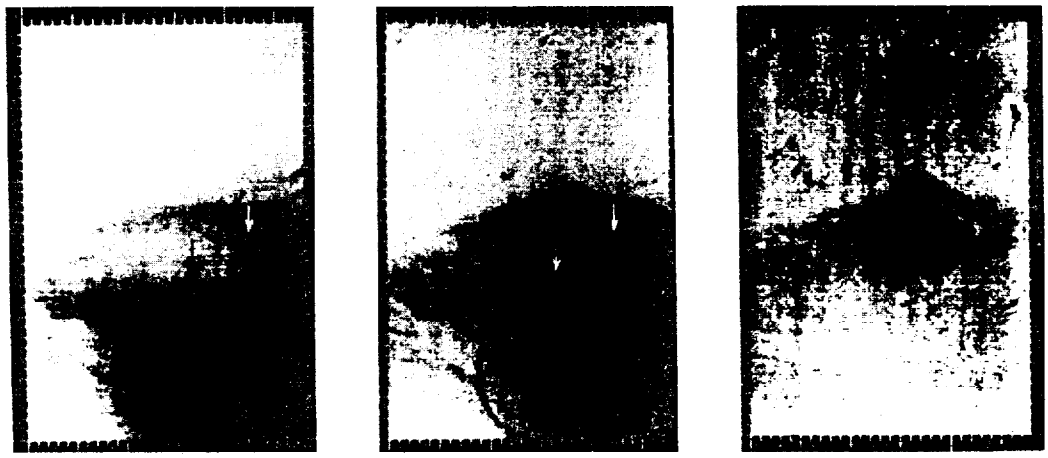

Fig. 26. Region of the two dark spots and the small channel shown in Figure 25. Left: revolution 125. Middle: revolution 160. The two views, similarly scaled and projected, were aligned relative to each other and differenced picture element by picture element to give the picture difference at right. Note the darkening in the vicinity of the two dark spots. Centered at 22.6°N, 64.5°W; width = 30 km (Stanford AIL Picture Product STN 0166, 042904).

Fig. 27. Wide-angle camera view of Promethei Sinus, centered at 71°S, 269°W, and about 750 km across. The solid outline shows the area of Figure 28 (MTVS 4211-9, DAS 08008038).

Figure 30 shows some of the significant changes that took place in region B after revolution 126. (Unfortunately, this region was not observed on revolution 99). In this region the splotch within the crater changed slightly between revolutions 126 and 179 and significantly between revolutions 181 and 220. In region D, however, changes occurred only between revolution 181 and 220 (Figure 32).

At the time of the formation of the leaf in region A, a strong change occurred in region C (top row of Figure 31). The change consisted in a general growth of the dark splotch both by the extension of the points on the scalloped edge and by the outward displacement of the amorphous edge. No subsequent changes were observed.

A sudden change in region E was observed between revolutions 181 and 220 (Figure 33), resulting in the extension of the points along the scalloped edge of the splotch. A similar change took place in region F at the same time (Figure 34).

A pattern of swift changes, interrupted by relatively long periods of quiescence, seems typical of Promethei Sinus. It is significant that regions A and C, which changed drastically between revolutions 99 and 126, did not participate in the major changes that affected the entire area between revolutions 181 and 220. A saturation effect seems to be involved. This major change affected surrounding areas, even at a scale detectable in low-resolution, wide-angle pictures (Figure 35).

WIND TUNNEL ANALOGS OF MARTIAN DUST TRANSPORT

A set of experiments possibly relevant to Martian eolian dust patterns was conducted by *Hertzler* [1966*a*, *b*] in the McDonnell Aircraft

Corporation's 14-foot environmental s
Ambient conditions were 5.35–26.7 mb
and room temperature. Two specimens
ing Martian surface material were used
flour with particle diameters largely
between 1 and 100 μm, and a white su
with particle diameters largely rangi
100 to 700 μm. Piles of these powders
cm thick were placed on smooth a
plates at the orifice of a wind tun
velocities measured were at an altitud
the surface boundary layer and ranged
m/sec. The resulting morphology of wi
dust apparently depended much more
cle size and layer thickness than up
velocity.

In Figure 36 are shown before a
photographs of a layer of sugar sand ex
these winds for about 100 min. Here a

Fig. 28. Narrow-angle camera view
is about 80 km across and is centered
following figures (MTVS 4213-12, DAS

ered at 71°S, 269°W, and about
(MTVS 4211-9, DAS 08008038).

ge of the splotch. A similar change
region F at the same time (Figure

of swift changes, interrupted by
ng periods of quiescence, seems
omethei Sinus. It is significant that
nd C, which changed drastically
olutions 99 and 126, did not partic-
major changes that affected the
etween revolutions 181 and 220. A
ffect seems to be involved. This
e affected surrounding areas, even
detectable in low-resolution, wide-
s (Figure 35).

Tunnel Analogs of Martian Dust Transport

experiments possibly relevant to
an dust patterns was conducted by
ibid., b] in the McDonnell Aircraft

Corporation's 14-foot environmental simulator. Ambient conditions were 5.35–26.7 mb pressure and room temperature. Two specimens simulating Martian surface material were used: a silica flour with particle diameters largely ranging between 1 and 100 μm, and a white sugar sand with particle diameters largely ranging from 100 to 700 μm. Piles of these powders about 1 cm thick were placed on smooth aluminum plates at the orifice of a wind tunnel. The velocities measured were at an altitude within the surface boundary layer and ranged up to 40 m/sec. The resulting morphology of windblown dust apparently depended much more on particle size and layer thickness than upon wind velocity.

In Figure 36 are shown before and after photographs of a layer of sugar sand exposed to these winds for about 100 min. Here a marked embayment is produced by the removal of bright material, revealing underlying dark material; the wind direction is into the figure, and the extent of the remaining bright material has decreased because of removal. Figure 37 shows a nearly identical experiment with a layer of silica flour exposed to these winds for about 100 min, but with the base plate inclined at an angle of 20°. Long streamers are produced opposite the direction of wind flow, possibly because of the backward gravitational displacement of particles. The scalloped material in Promethei Sinus resembles Figure 36 much more than Figure 37.

Figure 38 shows the results of an experiment performed on sugar sand for less than 10 min, but at velocities at the surface significantly above the threshold velocities for grain motion. The resulting pattern, like that in Figure 36

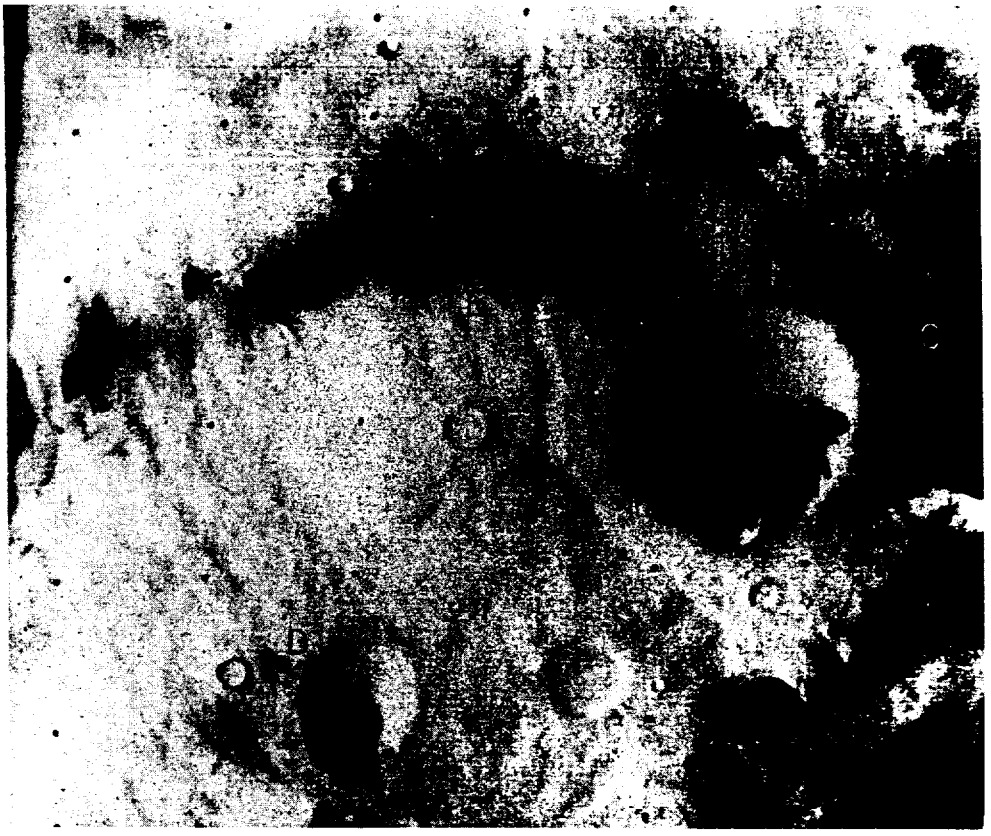

Fig. 28. Narrow-angle camera view of the region outlined (solid) in Figure 27. The picture is about 80 km across and is centered at 69.6°S, 253.1°W. Lettered regions are pictured in the following figures (MTVS 4213-12, DAS 08079893).

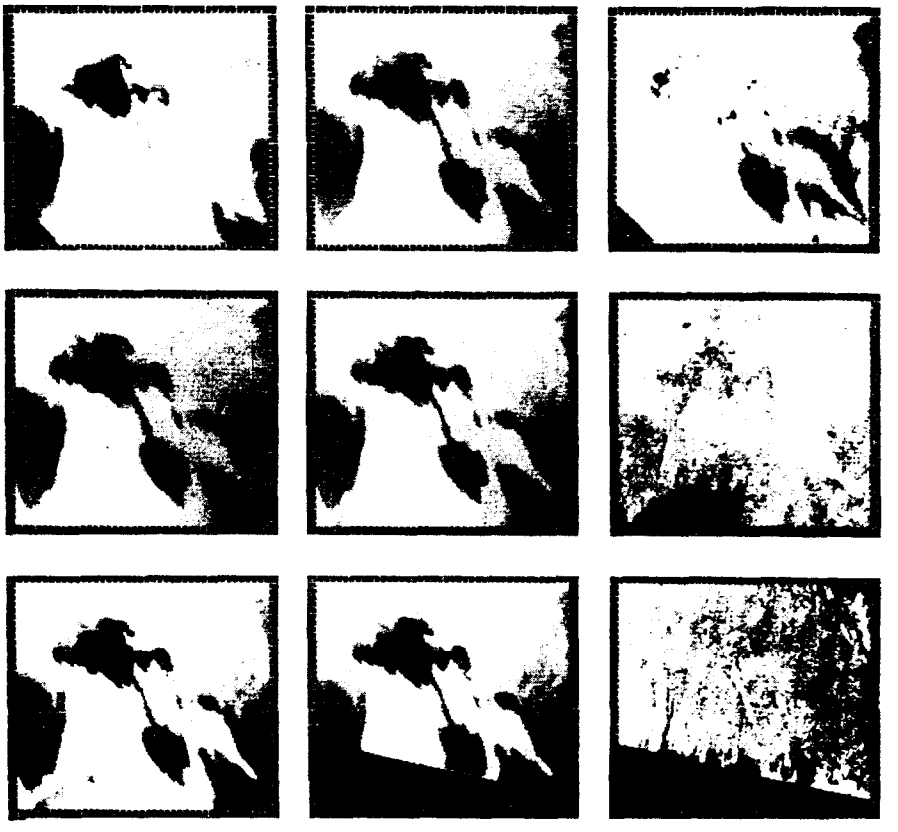

Fig. 29. Changes in region A. Top row (left to right): revolution 99, revolution 126, Stanford picture difference: revolution 126 minus revolution 99. Middle row: revolution 126, revolution 179, revolutions 179 minus 126. Bottom row: revolution 181, revolution 220, revolutions 220 minus 181. The window is about 20 km across, and is centered at 70.1°S, 253.3°W (Stanford AIL Picture Products STN 0167, 050609, 050610, 050611).

but unlike that in Figure 37, resembles Promethei Sinus.

The difference in scale is about 10°, and so the following comparison of wind tunnel and Martian eolian morphologies must be treated with some caution. From the optical depth of the great 1971 dust storm, the precipitated thickness of atmospheric particulates is easily estimated to be about 1 mm. Thus the thin layers being removed in the wind tunnel experiments are not inappropriate to the Martian case.

As time passes in Figure 37 it seems likely that, as more and more sand is removed, the dark indentations will grow windward with time. If this is an appropriate analog of the growth of scallops in Promethei Sinus (Figure 28), however, it implies bright material being driven by winds in precisely the sense opposite that indicated by the adjacent crater splotch (Figure 30). We therefore lean to the alternative view that the scallops are generated by winds blowing from the straight to the scalloped edge, consistent with the crater splotch reading. This requires dark rather than bright mobile material, or it might be accomplished by the preferential denudation of overlying bright material from the points of the scallops, perhaps because the underlying dark material is very smooth, as in a vitreous lava flow. The discontinuous appearance of the leaf in 13 days with no subsequent alteration strongly suggests a saturation phenomenon of the sort specifically anticipated in windblown dust models [*Sagan and Pollack*, 1969] for cases of the removal of overlying bright material from underlying dark. This supports the last explanation. Nevertheless, it is unfortunate that, with in
available both on the motion of th
and the direction of the prevailing
are still at this time unable to decid
it is bright or dark mobile materi
primarily responsible for the pheno
served in Promethei Sinus.

CLASSICAL VARIABLE FEATURES FRO MARINER 9 PERSPECTIVE

Certain secular changes can be cor
Martian topography, while no convin
graphic connection can be found for

In the first category is the dar
Phasis in 1877–1879 [*Antoniadi*, 19
Solis Lacus. The area affected is a
extension of rugged terrain into the
smooth region of Solis Lacus (cf. Fig

The smoothness and isolation of

Fig. 30. Changes in region B.
revolutions 179 minus 126. Middle
179. Bottom row: revolution 181,
about 20 km across and is centered
0173, 061109, 061110, 061111).

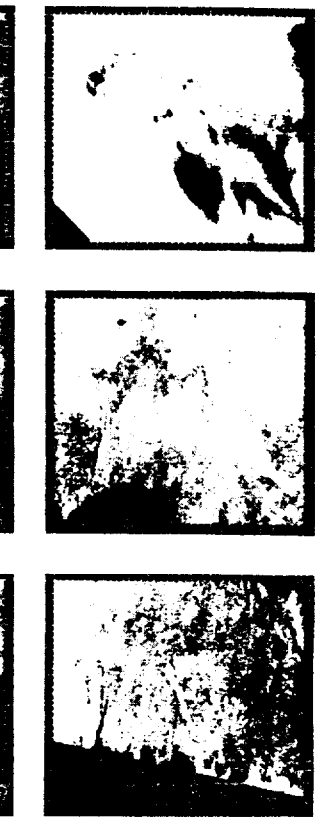

): revolution 99, revolution 126.
n 99. Middle row: revolution 126,
revolution 181, revolution 220,
ıcross, and is centered at 70.1°S,
99, 050610, 050611).

ıted by the adjacent crater splotch
). We therefore lean to the alterna-
that the scallops are generated by
ing from the straight to the scalloped
stent with the crater splotch reading.
es dark rather than bright mobile
r it might be accomplished by the
deviation of overlying bright
om the points of the scallops, per-
se the underlying dark material is
h, as in a vitreous lava flow. The
us appearance of the leaf in 13 days
sequent alteration strongly suggests
phenomenon of the sort specifically
in windblown dust models [*Sagan*
, 1969] for cases of the removal of
right material from underlying dark.
rts the last explanation. Neverthe-

less, it is unfortunate that, with information available both on the motion of the scallops and the direction of the prevailing winds, we are still at this time unable to decide whether it is bright or dark mobile material that is primarily responsible for the phenomena observed in Promethei Sinus.

CLASSICAL VARIABLE FEATURES FROM THE MARINER 9 PERSPECTIVE

Certain secular changes can be correlated to Martian topography, while no convincing topographic connection can be found for others.

In the first category is the darkening of Phasis in 1877–1879 [*Antoniadi*, 1930] near Solis Lacus. The area affected is a wedgelike extension of rugged terrain into the otherwise smooth region of Solis Lacus (cf. Figure 3).

The smoothness and isolation of the Solis Lacus region explains its susceptibility to secular changes [*Antoniadi*, 1930; *Pollack and Sagan*, 1967], especially when it is realized that the dark streaks are responsible for the major albedo markings in the area (see Figure 5).

Generally speaking, albedo markings are not closely correlated with topography: albedo markings are quite superficial. There are, however, a few interesting trends: large depressions such as the Coprates rift valley and the enclosed depression Juventae Fons tend to appear as dark albedo features from earth. In the Coprates rift valley, one can invoke scouring of fines by channeled winds as in the Lunae Palus canyon, but what is the explanation for Juventae Fons?

Also, in general, strong secularly variable features tend to lie in smooth regions. Examples are the Solis Lacus region and Syrtis Major

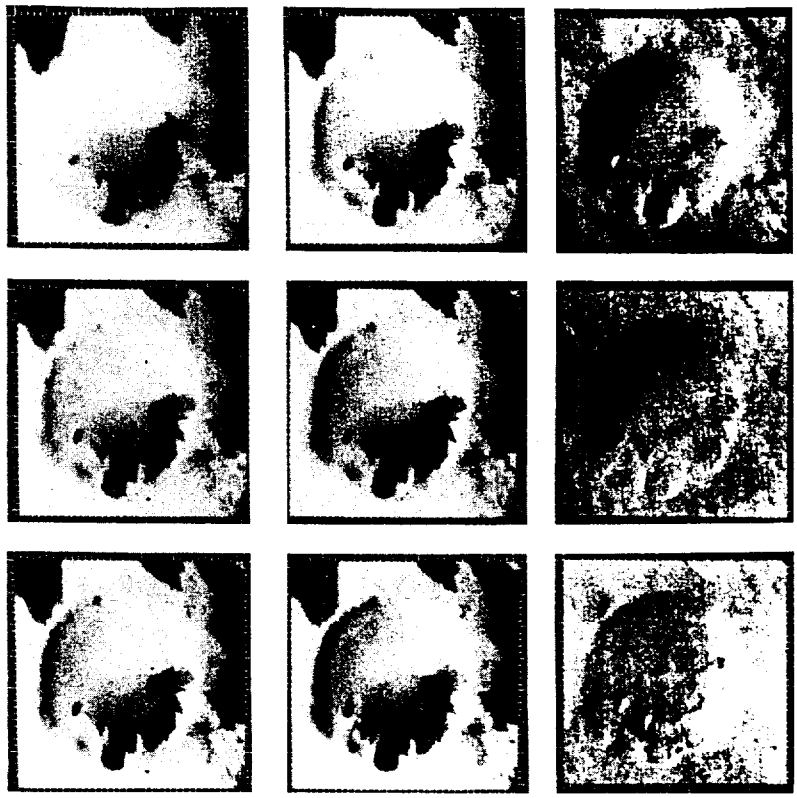

Fig. 30. Changes in region B. Top row (left to right): revolution 126, revolution 179, revolutions 179 minus 126. Middle row: revolution 179, revolution 181, revolutions 181 minus 179. Bottom row: revolution 181, revolution 220, revolutions 220 minus 181. The window is about 20 km across and is centered at 69.9°S, 253.7°W (Stanford AIL Picture Products STN 0173, 061109, 061110, 061111).

itself. The western stable edge of Syrtis Major is determined by topography. The eastern edge lies on a smooth sloping plane and is defined by dark, variable crater tails.

One of the most famous secular variations in the annals of Martian observations is the change in Hydaspes [*Antoniadi*, 1930]. This feature has lapsed into insignificance after being a prominent dark band joining Margaritifer Sinus to Niliacus Lacus from 1858 to 1871. Its trend corresponds closely to that of several channels running through the collapsed chaotic terrain into Chryse. This is a good example of a topographically controlled secular change.

On the other hand, no topographic control is evident in the strong darkening observed in Noachis in 1928 by *Antoniadi* [1930]. The region affected by this change is identical topographically to surrounding features that were not affected.

It has been claimed [*Boyce and Thompson*, 1972; W. Baum, private communication, 1972] on the basis of recent earth-based observations that, contrary to the classical view, Martian seasonal changes involve variations in the bright rather than the dark areas. We find, for the Mariner 9 season, no evidence to support this claim. Motion of dark splotches, development of dark streaks, and the filling in with dark material of bright intercrater regions have all been

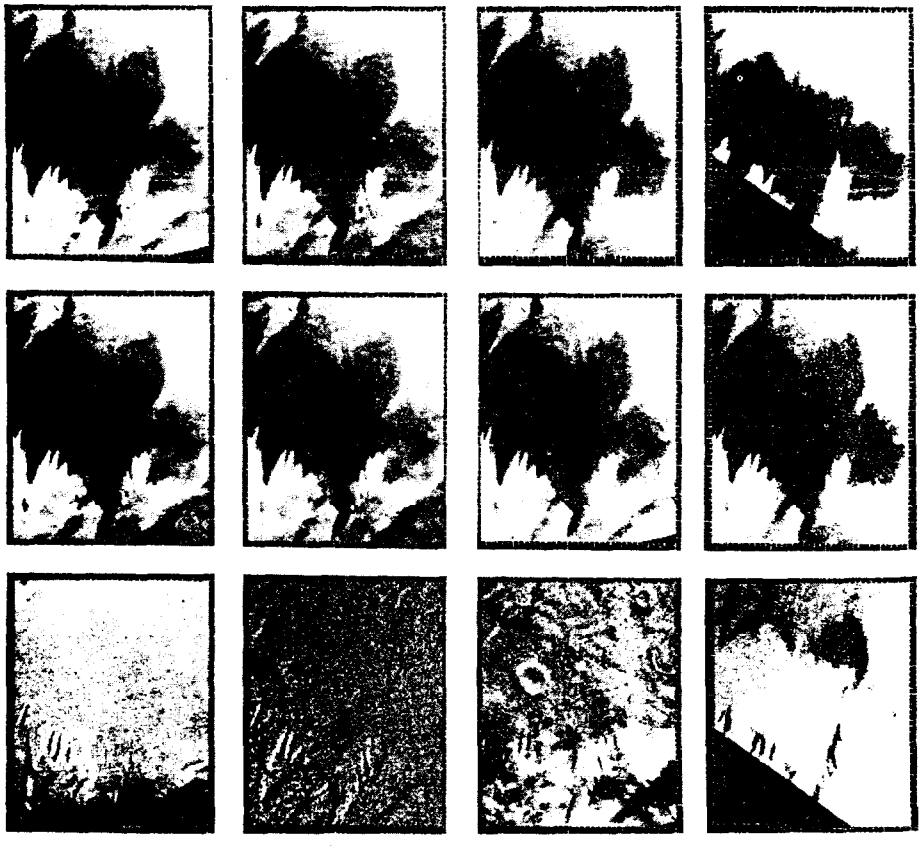

Fig. 31. Changes in region C. First row (top to bottom): revolution 99, revolution 126, revolutions 126 minus 99. Second row: revolution 126, revolution 179, revolutions 179 minus 126. Third row: revolution 179, revolution 181, revolutions 181 minus 179. Fourth row: revolution 181, revolution 220, revolutions 220 minus 181. The window is about 45 km across and is centered at 70.3°S, 254.2°W (Stanford AIL Picture Products STN 0173, 061105, 061106, 061107, 061108).

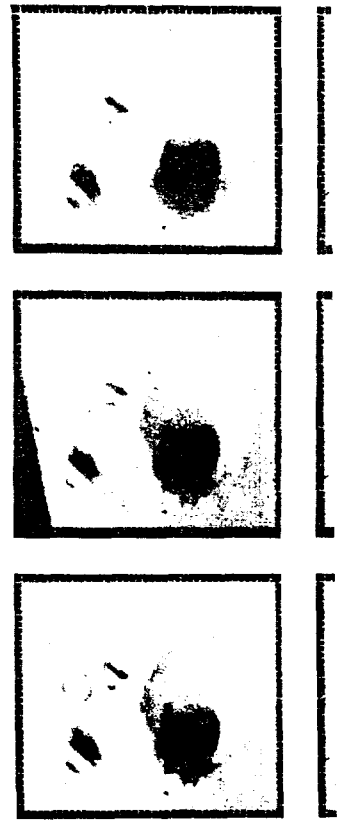

Fig. 32. Changes in region D. T
revolutions 181 minus 126. Middle r
179. Bottom row: revolution 181, r
about 20 km across and is centered
0173, 061101, 061102, 061103).

seen, while corresponding developments
features have not been observed. Hov
was pointed out in paper 1, such a tren
continue indefinitely if Mars is to mai
mean albedo. Comparison with Marin
7 results and Viking orbiter observati
uncover development of bright materi
complementary seasons. We suspect t
bright and dark materials are transp
Mars.

RATES OF DUST TRANSPORT

From the foregoing data, we deri
simple results on the rates of lateral t
of dust on Mars at times other tha
major dust storms. The material trar
the leaf region of Promethei Sinus am

SSION

in the strong darkening observed
in 1928 by *Antoniadi* [1930]. The
cted by this change is identical topo-
to surrounding features that were
l.

een claimed [*Boyce and Thompson,*
Baum, private communication, 1972]
is of recent earth-based observations
ary to the classical view, Martian
anges involve variations in the bright
n the dark areas. We find, for the
season, no evidence to support this
ion of dark splotches, development
eaks, and the filling in with dark ma-
ight intercrater regions have all been

a): revolution 99, revolution 126,
lution 179, revolutions 179 minus
ns 181 minus 179. Fourth row:
he window is about 45 km across
robuets STN 0173. 061105. 061106,

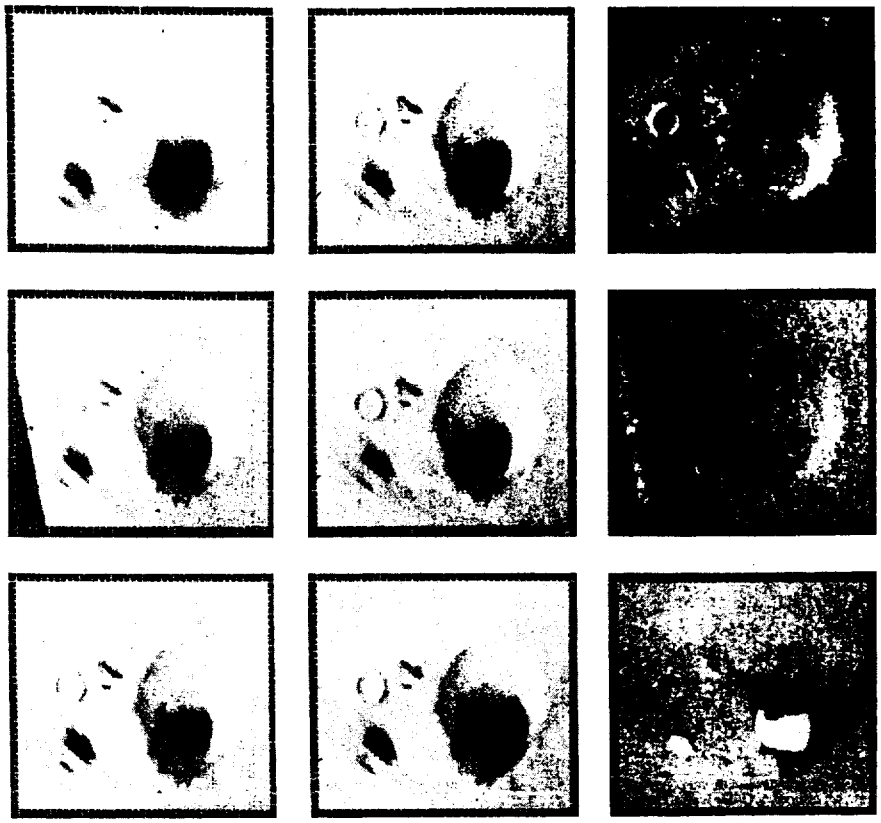

Fig. 32. Changes in region D. Top row (left to right): revolution 126, revolution 181, revolutions 181 minus 126. Middle row: revolution 179, revolution 181, revolutions 181 minus 179. Bottom row: revolution 181, revolution 220, revolutions 220 minus 181. The window is about 20 km across and is centered at 69.3°S, 252.7°W (Stanford AII, Picture Products STN 0173. 061101, 061102, 061103).

seen, while corresponding developments of bright features have not been observed. However, as was pointed out in paper 1, such a trend cannot continue indefinitely if Mars is to maintain its mean albedo. Comparison with Mariner 6 and 7 results and Viking orbiter observations may uncover development of bright material in the complementary seasons. We suspect that both bright and dark materials are transported on Mars.

Rates of Dust Transport

From the foregoing data, we derive some simple results on the rates of lateral transport of dust on Mars at times other than during major dust storms. The material transport in the leaf region of Promethei Sinus amounts to about 2 km in time intervals ≤ 19 days. Taking a threshold velocity of about 2 m sec, the prevailing winds transporting the mobile dust must blow for about 10^3 sec (about 15 min) in ≤ 19 days. Some of the streaks are several hundred kilometers long. If we assume that streak material is transported only at V_{*t}, this implies occasional strong prevailing winds of this velocity, with no significant dissipative currents for about 1 day out of several hundred. If the dust is carried higher in the boundary layer, the time scale for a pronounced directionality of strong winds can be even less. The continuity of the streaks, unaffected by local topography, argues for nonlocal transport, possibly high in the boundary layer; the remarkable straightness of the streaks argues for high winds with a

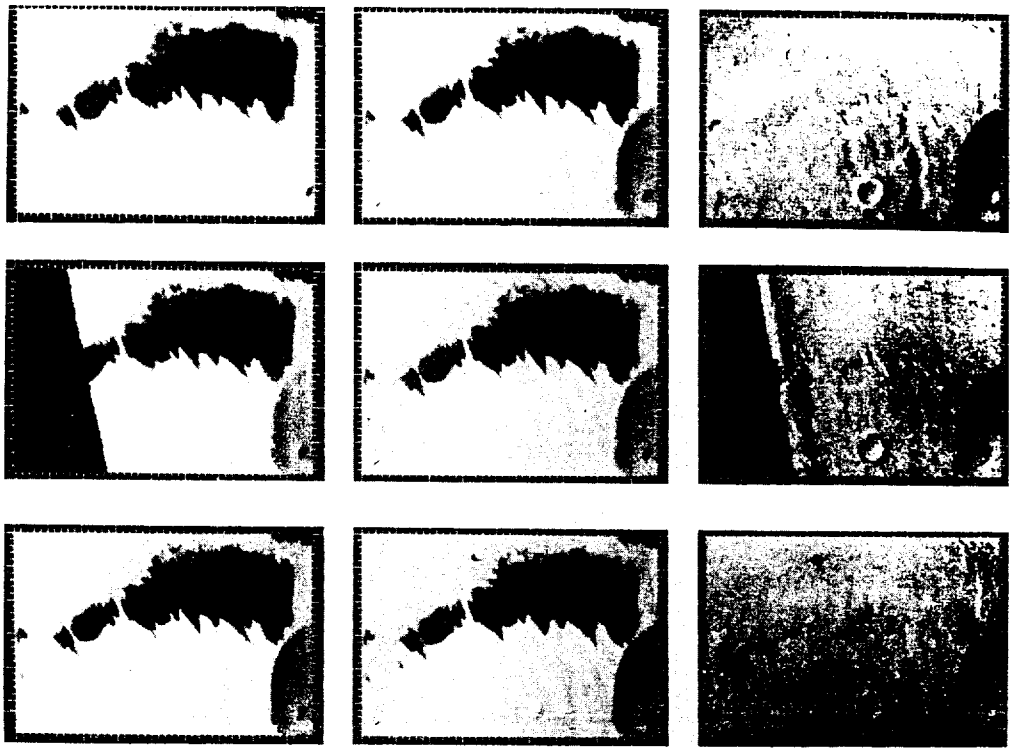

Fig. 33. Changes in region E. Top row (left to right): revolution 126, revolution 181, revolutions 181 minus 126. Middle row: revolution 179, revolution 181, revolutions 181 minus 179. Bottom row: revolution 181, revolution 220, revolutions 220 minus 181. The window is about 45 km across and is centered at 69.8°S, 252.5°W (Stanford AIL Picture Products STN 0173, 061112, 061113, 061114).

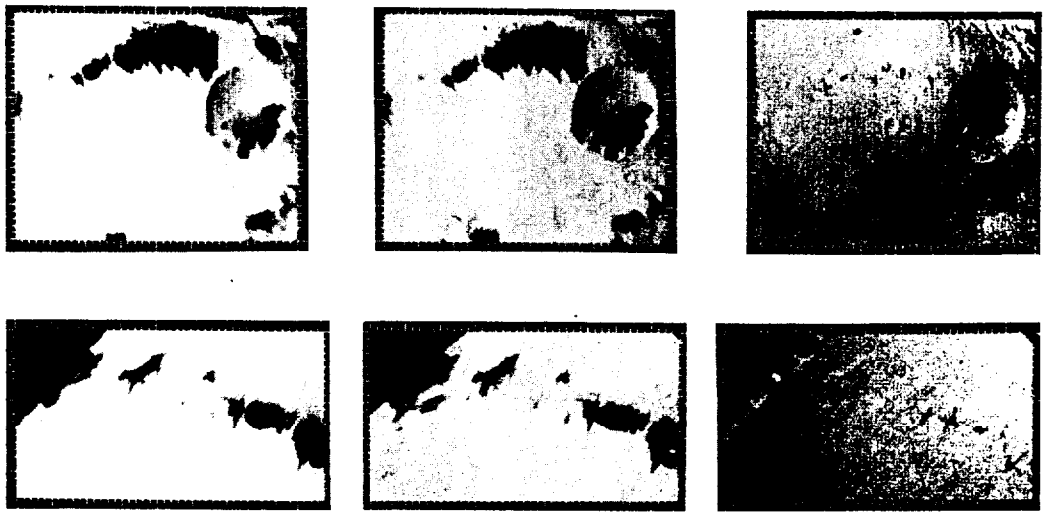

Fig. 34. Changes in region F are shown in the bottom row. Left to right: revolution 181, revolution 220, revolutions 220 minus 81. This window is about 40 km across and is centered at 69.6°S, 251.8°W (Stanford AIL Picture Product STN 0173, 061104). The top row shows changes in regions B, D, E over the same time interval. Left to right: revolution 181, revolution 220, revolutions 220 minus 181. The top window is about 60 km across, and is centered at 69.6°S, 253.1°W (Stanford AIL Picture Product STN 0166, 042905).

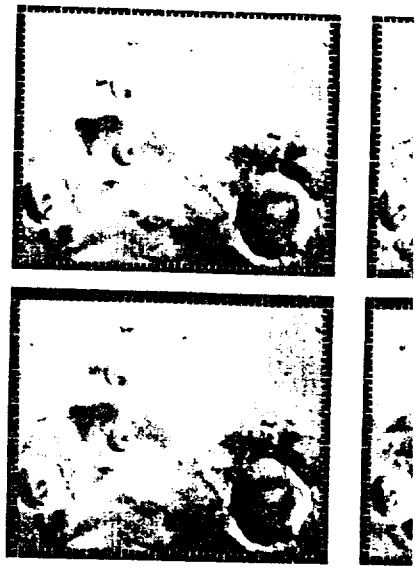

Fig. 35. Changes at wide-angle re
revolution 179, revolution 181, revolu
tion 220, revolutions 220 minus 179.
72.4°S, 267.2°W; its outline is show
STN 0174, 061306, 061307).

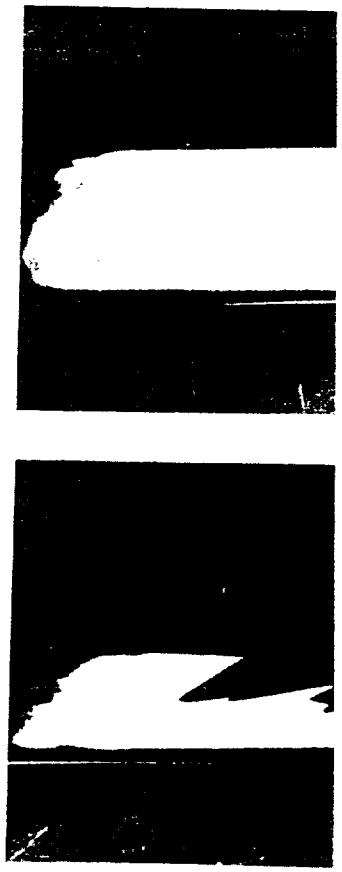

Fig. 36. Photographs of a layer
($\lesssim$40 m/sec) for 100 min: (*a*) before
Hertzler, 1966*a*, *b*].

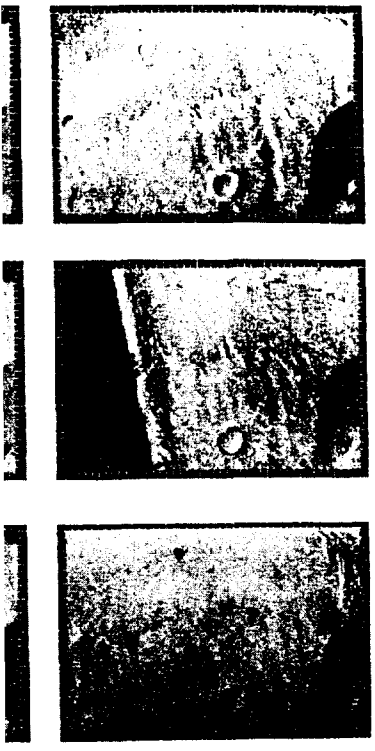

: revolution 126, revolution 181, olution 181, revolutions 181 minus is 220 minus 181. The window is nford AIL Picture Products STN

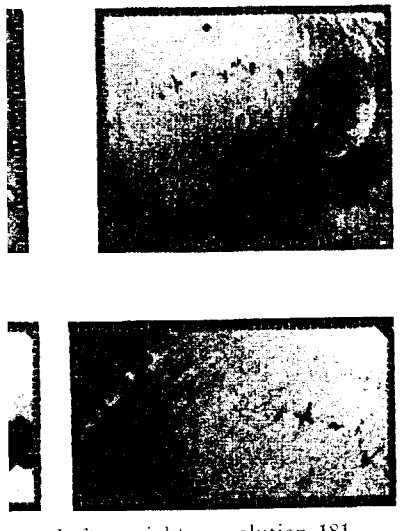

ow. Left to right: revolution 181, nt 40 km across and is centered at 31101). The top row shows changes ht; revolution 181, revolution 220, across, and is centered at 69.6°S,

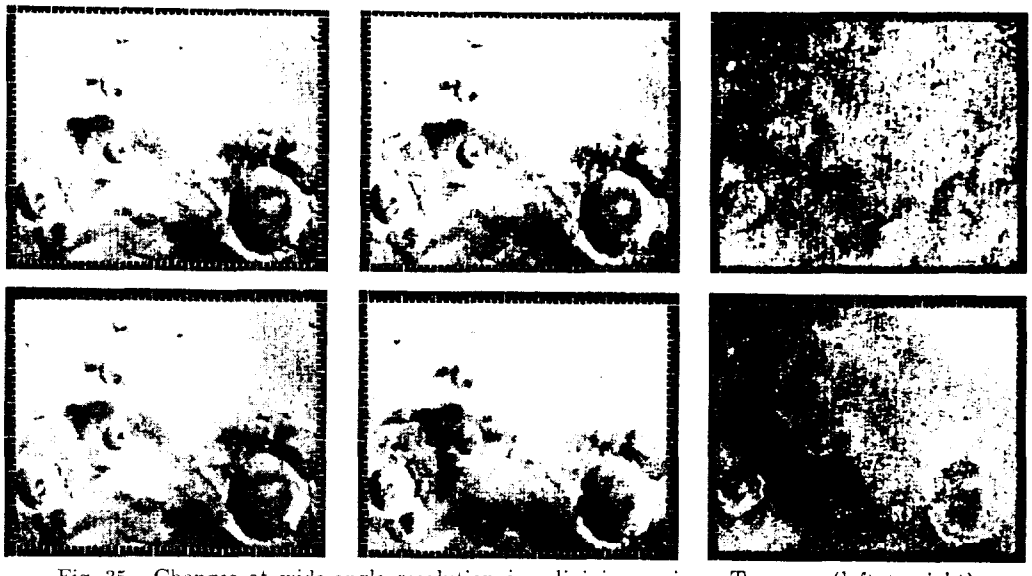

Fig. 35. Changes at wide-angle resolution in adjoining regions. Top row (left to right): revolution 179, revolution 181, revolutions 181 minus 179. Bottom row: revolution 179, revolution 220, revolutions 220 minus 179. The window is about 220 km across and is centered at 72.4°S, 267.2°W; its outline is shown dashed in Figure 27 (Stanford AIL Picture Products STN 0174, 061306, 061307).

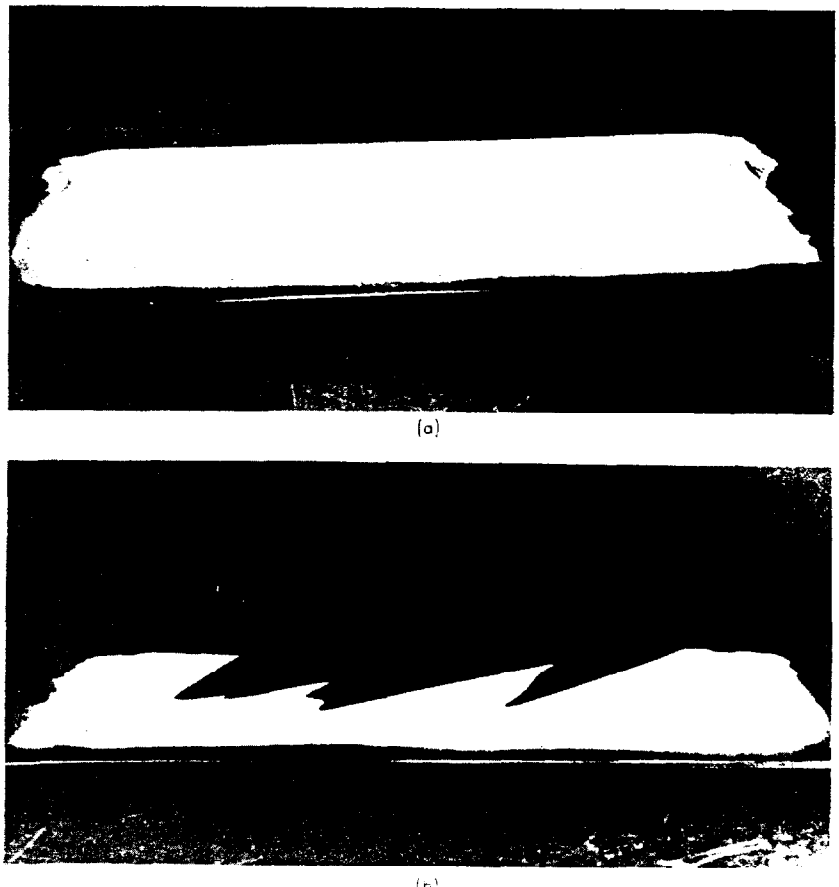

Fig. 36. Photographs of a layer of sugar (a)/sand (b) exposed to simulated Martian winds (≲40 m/sec) for 100 min: (*a*) before; (*b*) after. Wind direction is into the picture [from *Hertzler*, 1966*a*, *b*].

strong prevailing character for about 1 day, not an unlikely requirement.

On earth saltating particles can induce creep in surface grains many times their own diameter. For Mars the diameter ratio should be even larger. Thus small bright particles can induce creep in large dark particles. On earth, typical sandstorm creep velocities are about 1 cm/sec [*Bagnold*, 1954]; on Mars they should be correspondingly larger. Thus, during 1 day on Mars, creep of about 1 km is possible. It is curious, therefore, that the same velocities for the same periods of time can account by saltation for the production of bright streaks and by creep for the motions of dark material in places like Promethei Sinus.

Hertzler [1966*b*] estimated eolian transport rates under typical Martian conditions when the threshold stress is exceeded. Typical values range from 3×10^{-3} g cm^{-2} sec^{-1} to 3×10^{-5} g cm^{-2} sec^{-1}. Thus a layer of dust 1 cm thick could easily be removed in 1 Martian day under conditions of moderately high winds, a result quite consistent with that just derived on the time scale for the generation of streaks. These numbers imply typical dust removal rates for an area the size of the leaf in Promethei Sinus of about 100 tons/sec, most of which, being in saltating particles, will be immediately redeposited.

Deflation of dust out of gravitational potential wells such as craters probably requires velocities $> V_{*t}$; in this case also transport times are reduced. The high values of V_{*t} deduced here and elsewhere have important consequences for eolian erosion rates on Mars, as is discussed in a separate publication.

The contrasts that we find between adjacent

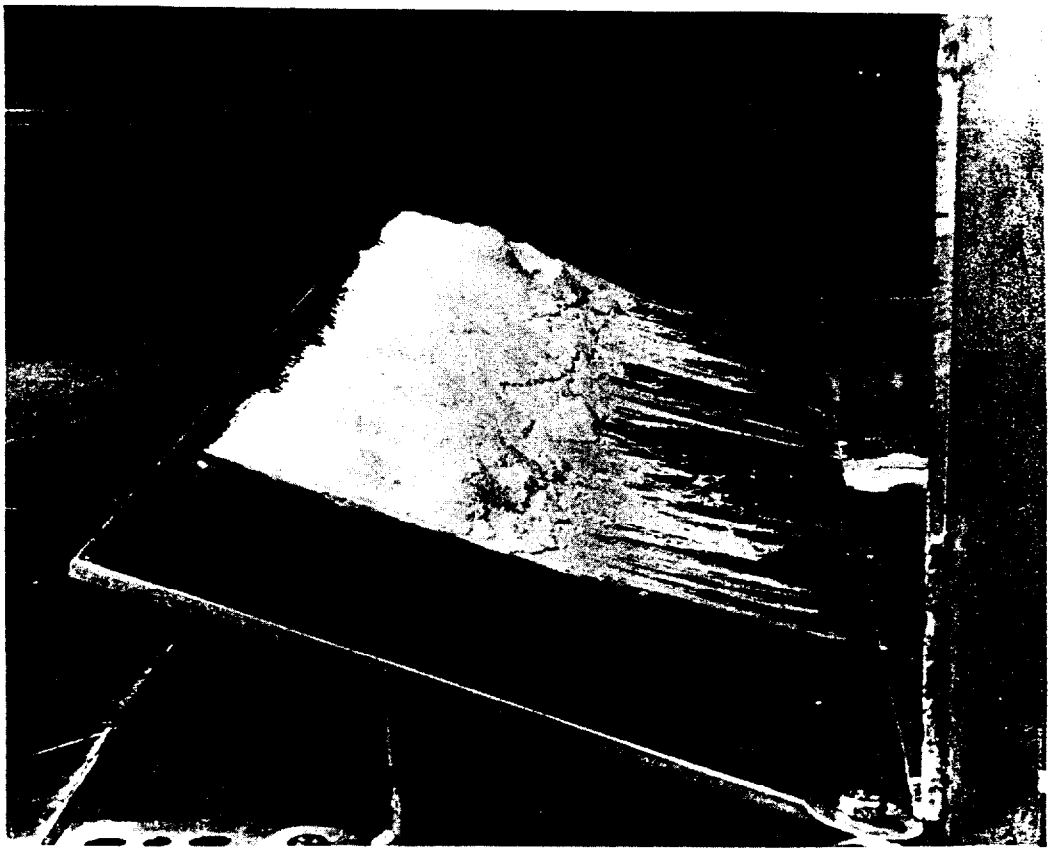

Fig. 37. Results of a wind tunnel experiment similar to that in Figure 36, but with the base plate inclined at 20° to the wind. Wind direction is from right to left [from *Hertzler*, 1966*a*, *b*].

Fig. 38. Results of a wind tur sand was exposed for ~10 min velocity needed to initiate grai *Hertzler*, 1966*a*, *b*].

bright and dark terrain, $\lesssim 20\%$, n either to composition differences, size differences, or to both. The two may indeed be connected through weathering of small particles [*Sa* 1971].

The apparent generation of brigh some Martian areas only as a re global dust storm (paper 1) sug bright streaks require exceptionally ties for their formation. According bright streak particles would be s below the most easily saltated p i.e., $\ll 100$ μm (cf. paper 1). This explains the otherwise puzzling fact cases of the development of dark splotches have been uncovered since of the great 1971 storm, but no c

3×10^{-3} g cm^{-2} sec^{-1} to 3×10^{-5} g
Thus a layer of dust 1 cm thick
be removed in 1 Martian day under
of moderately high winds, a result
stent with that just derived on the
for the generation of streaks. These
nply typical dust removal rates for
size of the leaf in Promethei Sinus of
tons/sec, most of which, being in
particles, will be immediately rede-

of dust out of gravitational poten-
such as craters probably requires
$> V_{*t}$; in this case also transport
reduced. The high values of V_{*t}
ere and elsewhere have important
es for eolian erosion rates on Mars,
ssed in a separate publication.
trasts that we find between adjacent

to that in Figure 36, but with the
from right to left [from *Hertzler,*

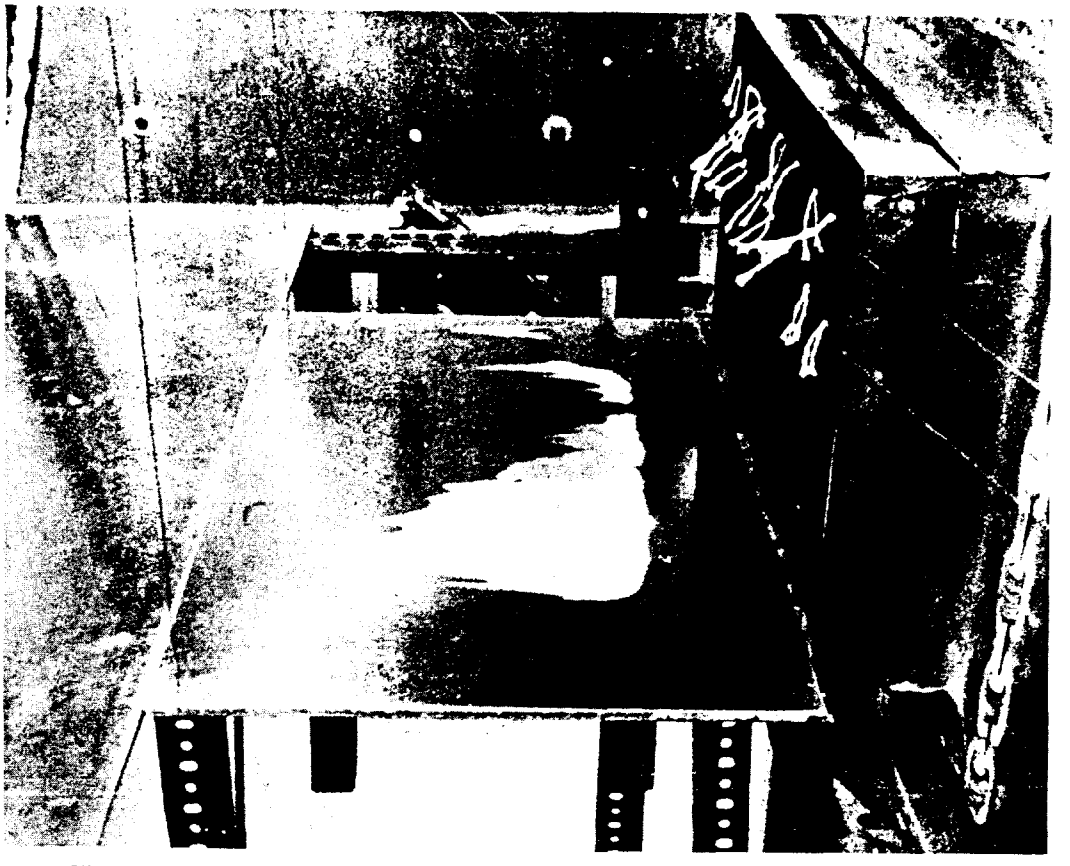

Fig. 38. Results of a wind tunnel experiment similar to that in Figure 36. Here the sugar sand was exposed for ~10 min to wind velocities significantly in excess of the threshold velocity needed to initiate grain movement. Wind direction is from right to left [from *Hertzler,* 1966*a*, *b*].

bright and dark terrain, $\lesssim 20\%$, may be due either to composition differences, to particle size differences, or to both. The two differences may indeed be connected through preferential weathering of small particles [*Sagan et al.*, 1971].

The apparent generation of bright streaks in some Martian areas only as a result of the global dust storm (paper 1) suggests that bright streaks require exceptionally high velocities for their formation. Accordingly, typical bright streak particles would be significantly below the most easily saltated particle size, i.e., $\ll 100$ μm (cf. paper 1). This deduction explains the otherwise puzzling fact that many cases of the development of dark streaks and splotches have been uncovered since the settling of the great 1971 storm, but no cases of the development of bright material have been detected. The high stability of the bright streaks is expected for an array of particles with threshold velocities far above the minimum V_{*t}, but the bright streak regions must be free of larger particles with threshold velocities near the minimum V_{*t}; saltation of such larger particles would, by momentum exchange, set the smaller particles of the bright streaks into suspension. Likewise dark areas are darkened when larger saltating particles eject smaller bright fines, which are then carried off in suspension.

Acknowledgments. We are grateful to R. A. Hand and J. A. Pirraglia for permission to reproduce here some of their Iris atmospheric circulation results; to W. Green, J. Seidman, R. Ruiz, and A. Schwartz for invaluable help with the picture processing; to R. Becker for interfacing;

to A. T. Young, B. A. Smith, C. Leovy, and J. McCauley for useful discussions; and to the scientists and engineers of the Jet Propulsion Laboratory who made this mission possible. All picture differencing in this paper was performed by Lynn Quam and the staff of Stanford's Artificial Intelligence Laboratory.

REFERENCES

Antoniadi, E. M., *La Planete Mars*, Hermann, Paris, 1930.

Bagnold, R. A., *The Physics of Blown Sand and Desert Dunes*, Methuen, London, 1954.

Blumsack, S. L., On the effects of large scale temperature advection in the Martian atmosphere, *Icarus, 15*, 429, 1971.

Boyce, P. B., and D. T. Thompson, A new look at the Martian violet haze problem, 1. Arabia-Syrtis Major, *Icarus, 16*, 291, 1972.

Conrath, B., R. Curran, R. Hanel, V. Kinde, W. Maguire, J. Pearl, J. Pirraglia, J. Welker, and T. Burke, Atmospheric and surface properties of Mars obtained by infrared spectroscopy on Mariner 9, *J. Geophys. Res., 78*, this issue, 1973.

de Vaucouleurs, G., *Physics of the Planet Mars*, Faber and Faber, London, 1954.

Dollfus, A., New optical measurements of planetary diameters, 4, The north pole of Mars, *Icarus, 18*, 142, 1973.

Focas, J. H., Etude photometrique et polarimetrique des phenomenes saisonniers de la planete Mars, *Ann. Astrophys., 24*, 309, 1961.

Gierasch, P., and R. Goody, A model of a Martian great dust storm, *J. Atmos. Sci., 30*, 169, 1973.

Gierasch, P., and C. Sagan, A preliminary assessment of Martian wind regimes, *Icarus, 14*, 312, 1971.

Golitsyn, G. S., Martian dust storms, *Icarus, 18*, 113, 1973.

Hanel, R., B. Conrath, W. Hovis, V. Kunde, P. Lowman, W. Maguire, G. Levin, P. Straat, and T. Burke, Investigation of the Martian environment by infrared spectroscopy on Mariner 9, *Icarus, 17*, 423, 1972.

Hertzler, R. G., Particle behavior in a simulated Martian environment, *Rep. E720*, McDonnell Aircraft Corp., Huntington Beach, Calif., 1966*a*.

Hertzler, R. G., Behavior and characteristics of simulated Martian sand and dust storms, *Rep. E720*, McDonnell Aircraft Corp., Huntington Beach, Calif., 1966*b*.

Hess, S., Martian winds and dust clouds, paper presented at NATO Advanced Study Institute on Planetary Atmospheres, Istanbul, 1972.

Leovy, C., and Y. Mintz, Numerical simulation of the atmospheric circulation and climate of Mars, *J. Atmos. Sci., 26*, 1167, 1969.

Leovy, C., G. Briggs, A. T. Young, B. A. Smith, J. Pollack, E. Shipley, and R. Wildey, Mariner 9 television experiment: Progress report on studies of the Mars atmosphere, *Icarus, 17*, 373, 1972.

Leovy, C., R. Zurek, and J. Pollack, Mechanisms for Mars dust storms, *J. Atmos. Scis.*, in press, 1973.

Morris, E. C., T. A. Mutch, and H. E. Holt, Atlas of geologic features in the dry valleys of South Victoria Land, Antarctica, *Interagency Rep.: Astrogeol. 52*, U.S. Geol. Surv., Washington, D. C., 1972.

Pollack, J. B., and C. Sagan, Secular changes and dark-area regeneration on Mars, *Icarus, 6*, 434, 1967.

Sagan, C., and J. B. Pollack, A windblown dust model of Martian surface features and seasonal changes, *Smithson. Astrophys. Observ. Spec. Rep. 255*, 1967.

Sagan, C., and J. B. Pollack, Windblown dust on Mars, *Nature, 223*, 791, 1969.

Sagan, C., J. Veverka, and P. Gierasch, Observational consequences of Martian wind regimes, *Icarus, 15*, 253, 1971.

Sagan, C., J. Veverka, P. Fox, R. Dubisch, J. Lederberg, E. Levinthal, L. Quam, R. Tucker, J. B. Pollack, and B. A. Smith, Variable features on Mars: Preliminary Mariner 9 results, *Icarus, 17*, 346, 1972.

Smith, H. T. U., Eolian geomorphology, wind direction, and climatic change in North Africa, *Final Rep. AF contract 19(628)-298*, Bedford, Mass., 1963.

(Received February 7, 1973;
revised March 9, 1973.)